Potential role of strain hardening in the cessation of rifting at constant tectonic force

Tadashi Yamasaki, Randell Stephenson

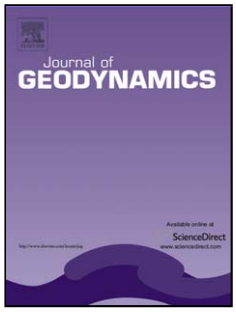

Title: Potential role of strain hardening in the cessation of rifting at constant tectonic force

Authors: Tadashi Yamasaki, Randell Stephenson

PII: S0264-3707(08)00060-4
DOI: doi:10.1016/j.jog.2008.07.001
Reference: GEOD 857

To appear in: *Journal of Geodynamics*

Received date: 22-1-2008
Revised date: 4-7-2008
Accepted date: 10-7-2008

Please cite this article as: Yamasaki, T., Stephenson, R., Potential role of strain hardening in the cessation of rifting at constant tectonic force, *Journal of Geodynamics* (2007), doi:10.1016/j.jog.2008.07.001

Potential role of strain hardening in the cessation of rifting at constant tectonic force

Tadashi Yamasaki and Randell Stephenson

Department of Tectonics, Faculty of Earth and Life Sciences, VU University Amsterdam, De Boelelaan 1085, 1081 HV Amsterdam, Netherlands.

All correspondence concerning this paper should be addressed to:
Tadashi Yamasaki
Department of Tectonics, Faculty of Earth and Life Sciences, VU University Amsterdam, De Boelelaan 1085, 1081 HV Amsterdam, Netherlands.
Tel: +31-20-5983921
Fax: +31-20-5989943
Email: tadashi.yamasaki@falw.vu.nl

Abstract

In this study the cessation of rifting at constant tectonic force is discussed from the view point of lithospheric rheology using a simple one-dimensional numerical model. The behaviour of the conventionally adopted constant force model re-examined in this study contradicts some general features in the development of sedimentary basins. Strain hardening is implemented to explain the contradictions, in which the viscosity of the mantle is a function of not only the strain rate and temperature but also the total strain. The roles of various strain hardening parameters in rifting dynamics are examined, including the strain required for the onset of hardening, the strain interval required for the completion of hardening and the factor controlling the increase in mantle viscosity. It is shown that a model with strain hardening can explain many characteristic features of sedimentary basin formation better than the conventional constant force model. There are a variety of ways in which rifting can be terminated by the strain hardening model, depending on the initial lithospheric structure, magnitude of tectonic force and the hardening process. One possible strain hardening mechanism involves the switch from wet to dry rheology associated with decompressional melting, though the implemented strain hardening formula could be generally applicable to any hardening phenomenon and could therefore be physically interpreted as such. The results of this study also provide important insights into sedimentary basin subsidence in relation to rifting dynamics. The end of an initial rapid ("syn-rift" like) subsidence phase is not necessarily equivalent to the end of actual rifting as in the constant force model. The transition from initial rapid subsidence to long-term, more subdued ("post-rift" like), subsidence is actually marked by the onset of deceleration of rifting. Since significant extension still continues for some time thereafter, the subsequent long-term subsidence includes some mechanical effect of crustal thinning.

Keywords: rifting; strain rate; stretching factor; tectonic subsidence; strain hardening; tectonic force

1. Introduction

The simple stretching model proposed by McKenzie (1978) and its modified models (e.g., Jarvis and McKenzie, 1980; Royden and Keen, 1980; Beaumont et al., 1982; Podladchikov et al., 1994; Yamasaki and Nakada, 1997) have been successful in explaining a style of subsidence that is generally characterized by an initial rapid phase and a subsequent long-term one (syn- and post-rift subsidence phases). However, such kinematic models are limited in their ability to provide insight into the dynamic aspects of rifting. Even though the degree of extension (typically quantified as a stretching- or β-factor) is one of the most important parameters describing the development of sedimentary basins, there is no clear answer to what controls it. Important relevant questions are why the rifting process does not always lead to continental break-up and seafloor spreading and what the physical processes are that lead to the cessation of rifting in a geologically reasonable manner.

Cessation of rifting can be discussed in terms of external or internal factors. The external factor is related to changes in the tectonic force that drives rifting in the first place. However, the origin of tectonic force and, therefore, what causes it to change, are also still poorly constrained. Interaction between plates play an important role in generating the driving forces (e.g., Forsyth and Uyeda, 1975; Uyeda and Kanamori, 1979; Bott, 1982; Le Pichon, 1983), but it is not well known how the forces operate on the continental lithosphere in an intraplate setting (e.g., Nielsen et al., 2007). What is known is that the available magnitude of extensional tectonic force is typically in the order of ~ 6 TN/m (e.g., Forsyth and Uyeda, 1975; Parsons and Richter, 1980; Bott et al., 1989; Bott, 1991; Schellart, 2004). Accordingly, it is also necessary to discuss the cessation of rifting in terms of internal factors such as intrinsic changes in lithospheric rheology given the widely accepted importance of rheological controls prior to and/or during rifting in a variety of extensional deformation styles (e.g., England, 1983; Braun and Beaumont, 1987; Kusznir and Park, 1987; Takeshita and Yamaji, 1990; Bassi, 1991; Buck, 1991; Govers and Wortel, 1993; Hopper and Buck, 1993; Bassi, 1995; Govers and Wortel, 1995; Newman and White, 1997; 1999; Frederiksen and Braun, 2001; Huismans and Beaumont, 2002; 2003).

This paper deals with the rheology-controlled cessation of rifting on the basis of a simple one-dimensional model that assumes constant tectonic force, in which the cessation of rifting requires an increase in lithospheric strength during extension. In previous models, this strengthening has been achieved only by thermal relaxation and replacement of crust with mantle (e.g., England, 1983; Takeshita and Yamaji, 1990; Hopper and Buck, 1993; Negredo et al., 1995; van Wijk and Cloetingh, 2002). The behaviour of the conventional constant force model is re-examined first to demonstrate that additional hardening mechanisms are indeed required to explain various observed configurations of sedimentary basin development. Then, an *ad hoc* strain hardening mechanism is introduced to the

model in order to explore some possible consequences, in which the viscosity of mantle is dependent not only on the strain rate and temperature but also on the total strain, and the roles of the parameters in this model in controlling the temporal evolution of strain rates and stretching factors are examined.

The model also allows the temporal evolution of tectonic subsidence to be investigated in relation to rifting dynamics. Although many studies have applied constant strain rates for a fixed duration of rifting in order to examine the behaviour of sedimentary basin subsidence (e.g., Jarvis and McKenzie, 1980), it is actually difficult to envisage how the magnitude of applied tectonic force can change conveniently to keep strain rate constant. Thus, it is perhaps also more reasonable to consider basin subsidence occurring in the presence of a constant force rather than imposing a constant strain rate. However, very few studies have dealt with tectonic subsidence in the context of a constant force model, focusing instead only on large-scale lithosphere deformation (e.g., Braun and Beaumont, 1987; Takeshita and Yamaji, 1990; Hopper and Buck, 1993; Govers and Wortel, 1993; 1995) or stress redistribution in the lithosphere (e.g., Kusznir, 1982; Ershov and Stephenson, 2006). One exception is the work of Newman and White (1997; 1999), in which rheology of the lithosphere was inferred by comparing strain rates inverted from observed basin subsidence with the behaviour of a constant tectonic force model.

2. Model description

The simple one-dimensional model adopted in this study is similar to that of Takeshita and Yamaji (1990) and Hopper and Buck (1993), except for the strain-dependent mantle viscosity. A schematic figure of the model is shown in Fig. 1. The entire lithosphere is extended in pure shear by an applied tectonic force F_a that is assumed to be constant over time. The lithosphere is assumed to consist of three layers: wet quartzite upper crust, anorthite lower crust and wet olivine mantle. The initial thickness of the entire crust is t_c and both the upper and lower crusts have thicknesses of $t_c/2$. The thickness of the thermal lithosphere (a) is defined by the depth of the 1350 °C isotherm. Strain hardening is introduced for the mantle only because the total strength of the lithosphere is mostly controlled by the strength of the mantle lithosphere (e.g., Kohlstedt et al., 1995).

Realistic two- or three dimensional models require the incorporation of lateral rheological heterogeneity prior to extension in order to localize extensional deformation in a particular region (e.g., Fernàndez and Ranalli, 1997), and, accordingly, rifting dynamics is strongly influenced by any assumed initial heterogeneity (e.g., Dunbar and Sawyer, 1988; Braun and Beaumont, 1989; Corti and Manetti, 2006; Corti et al., 2007; Yamasaki and Gernigon, 2008). However, in practice, it is difficult to deduce a given initial heterogeneity suitable for reproducing an actual rift structure. Therefore, in order to

avoid such difficulties, a simple one-dimensional model of the extensional evolution at the centre of a rift is adopted. Furthermore, the buoyancy force generated by the thinning of low-density crust is ignored, because this force is negligible compared to the tectonic force (e.g., Newman and White, 1999).

2.1 Lithospheric rheology

In the shallower parts of lithosphere, where temperature and pressure are low, deformation takes place in a brittle manner. The brittle stress σ_b is almost insensitive to rock type and temperature, being mainly a function of lithostatic pressure or depth (Byerlee, 1978; Goetze and Evans, 1979; Brace and Kohlstedt, 1980; Ranalli, 1995);

$$\sigma_b = \psi(1 - \upsilon^*)z \quad (1)$$

where ψ is the constant, υ^* is the density ratio of pore water to rock matrix and z is the depth.

At higher temperature and pressure, deformation takes place by ductile flow in response to an applied stress. In this study it is assumed that ductile deformation is controlled by dislocation creep (e.g., Carter and Tsenn, 1987):

$$\sigma_d = \left(\frac{\dot{\varepsilon}}{A^*}\right)^{\frac{1}{n}} \exp\left(\frac{Q}{nR\Gamma}\right) \quad (2)$$

where σ_d is the ductile stress, $\dot{\varepsilon}$ is the strain rate, A* is a material constant, Q is the activation energy, n is the power exponent of stress, R is the universal gas constant and Γ is the absolute temperature. Flow law parameters for each rock composition are shown in Table 1.

2.2 Thermal calculation

The ductile rheology is strongly sensitive to temperature, which is determined by solving the heat transport equation:

$$\frac{\partial T}{\partial t} = \kappa\frac{\partial^2 T}{\partial z^2} - \nu\frac{\partial T}{\partial z} + \frac{H}{\rho c} \quad (3)$$

where T is the temperature, t is the time, κ is the thermal diffusivity, z is the depth, ν is the vertical velocity of a material point, H is the amount of internal heating due to radioactive elements, ρ is the density and c is the specific heat. For pure shear thinning, the velocity ν increases linearly with depth as $\nu = \dot{\varepsilon}z$. It is noted that the reference frame moves with surface subsidence. Radioactive heat sources are assumed to be uniformly distributed in the entire crust but are neglected in the mantle. Eq. (3) is solved using an explicit finite difference method with the boundary condition that the temperature at the surface and bottom of the model is 0 and 1350 ºC, respectively. The initial temperature profile is

given by the steady state solution of Eq. (3) with $\nu = 0$. Parameter values used in the thermal calculation are shown in Table 1.

2.3 Strain rate calculation

The total strength of the thermal lithosphere (S) is calculated by the integration of the stress profile from the surface to base of the thermal lithosphere:

$$S = \int_0^a \sigma \, dz \tag{4}$$

where σ is given by the lesser of brittle stress σ_b and ductile stress σ_d at each depth. In the constant force model, the total strength S is always equal to the applied tectonic force F_a so that the strain rate $\dot{\varepsilon}$ is evaluated to satisfy the following equation at each time (Takeshita and Yamaji, 1990; Hopper and Buck, 1993):

$$F_a - S(\dot{\varepsilon}, t) = 0 \tag{5}$$

The calculation is terminated when the strain rate $\dot{\varepsilon}$ reaches 10^{-13} (s^{-1}), as such a high strain rate may be geologically unreasonable at the whole lithospheric scale (Martinez and Cochran, 1988).

2.4 Strain hardening formula: relationship between strain and viscosity

Strain hardening is introduced by means of an *ad hoc* relationship between viscosity and strain. A similar formulation has been applied for strain softening to investigate the strain localization during extensional deformation of crust and mantle lithosphere (Frederiksen and Braun, 2001; Huismans and Beaumont, 2002; 2003). From Eq. (2), the viscosity η can be written in the form

$$\eta = B^* \dot{\varepsilon}^{(1/n)-1} \exp\left(\frac{Q}{nR\Gamma}\right) \tag{6}$$

In order to introduce strain hardening it is assumed that B^* is controlled by an equation of the form:

$$B^* = B\{\theta + \delta(1-\theta)\} \tag{7}$$

where $B = (1/A^*)^{1/n}$ and δ is the factor controlling the increase in viscosity associated with strain hardening. θ decreases linearly from 1 to 0 as the strain ε increases:

$$\begin{cases} \theta = 1 & (\varepsilon \le \varepsilon_o) \\ \theta = 1 - \dfrac{\varepsilon - \varepsilon_o}{\Delta E} & (\varepsilon_o < \varepsilon < \varepsilon_o + \Delta E) \\ \theta = 0 & (\varepsilon \ge \varepsilon_o + \Delta E) \end{cases} \tag{8}$$

The behaviour of B^* is illustrated in Fig. 2. B^* is kept constant at B until ε reaches ε_o and then linearly

increases to δB over the strain interval ΔE. For ε more than $\varepsilon_o + \Delta E$, B^* is kept constant at δB. This parameterisation of strain hardening is not based on any particular hardening mechanism. However, it completely describes the rheological behaviour associated with the transition from weak to strong rheology, as pointed out by Frederiksen and Braun (2001).

2.5 Stretching factor and tectonic subsidence

The time-dependent stretching factor β is evaluated using the change in crustal thickness,

$$\beta = t_c / t_{ct} \tag{9}$$

where t_c is the initial crustal thickness and t_{ct} is the crustal thickness at time t. The temporal evolution of tectonic subsidence ζ (water loaded) is calculated using the equation

$$\zeta = \frac{\int_t \rho(z)(1-\alpha T(z))\,dz - \int_0 \rho(z)(1-\alpha T(z))\,dz}{\rho_m(1-\alpha T_a) - \rho_w} \tag{10}$$

where $\rho(z)$ and $T(z)$ is the depth-dependent density and temperature, respectively, α is the coefficient of thermal expansion, ρ_m is the density of mantle, T_a is the potential temperature of asthenosphere, and ρ_w is the density of water. The first and second term in the numerator in Eq. (10) indicates the mass of lithosphere at time t and zero, respectively.

3. Model results

3.1. Results of the reference conventional model (RCM)

Fig. 3 shows the temporal evolutions of strain rate ($\dot{\varepsilon}$), stretching factor (β) and tectonic subsidence (ζ), where the thickness of the thermal lithosphere (*a*) is assumed to be 90 km. Each curve in the figure represents a different magnitude of tectonic force (F_a). As discussed in previous studies (Takeshita and Yamaji, 1990; Hopper and Buck, 1993; Newman and White, 1997; 1999), the ultimate fate of rifting in the constant force model is generally classified into two modes, failure or break-up, which are controlled by the competition between weakening due to elevated geothermal gradient and strengthening due to thermal relaxation and replacement of crust with mantle. When F_a is beyond the critical value (F_{cu}), the rifting process leads to the break-up mode. In contrast, when F_a is less than F_{cu}, the rifting process results in the failure mode. A minimum critical tectonic force F_{cl}, below which no significant extension takes place, can be also defined. Thus, models with $F_{cl} \le F_a \le F_{cu}$ are those that produce sedimentary basins with finite stretching factors. F_{cl} and F_{cu} for a given lithosphere structure are summarized in Appendix A.

Figs 3(a) and (b) show $\dot{\varepsilon}$ as a function of time for models with an initial crustal thickness (t_c) of 30 and 40 km, respectively. In this study, following Newman and White (1997; 1999), the duration of

rifting (Δt_D) is defined as a period in which $\dot{\varepsilon}$ is more than 10^{-17} (1/s). Δt_D is predicted to be shorter for greater F_a. This is because strengthening by thermal relaxation and crustal thinning works more efficiently at higher $\dot{\varepsilon}$: the greater thermal anomaly brought about by higher $\dot{\varepsilon}$ results in a higher rate of thermal relaxation, and the replacement of the crust with the mantle also takes place more effectively for a higher $\dot{\varepsilon}$. However, Δt_D is rarely predicted to be less than 53 and 40 my for models with t_c = 30 and 40 km, respectively.

Figs 3(c) and (d) show β as a function of time for models with t_c = 30 and 40 km, respectively. β does not increase significantly for $\dot{\varepsilon}$ less than 10^{-17} (1/s). This is consistent with the definition of Δt_D as the period in which $\dot{\varepsilon}$ is greater than 10^{-17} (s^{-1}). Potential finite β increases as F_a increases. However, finite values of β are restricted to be less than 1.55 and 1.60 for the models with t_c = 30 and 40 km, respectively. Thus, in the RCM, β is either less than these fairly low values or is infinite.

Figs 3(e) and (f) show tectonic subsidence (ζ) as a function of time for models with t_c = 30 and 40 km, respectively. ζ increases as crustal thinning progresses (the so-called initial subsidence or syn-rift subsidence). However, once $\dot{\varepsilon}$ decelerates to less than 10^{-17} (1/s), ζ is controlled chiefly by thermal relaxation (the so-called post-rift thermal subsidence). For the model with t_c = 30 km, the transition from rapid initial subsidence to subsequent long-term subsidence is not clearly perceptible. On the other hand, for the model with t_c = 40 km, the transition between the two phases is rather clear. An inflection point on the subsidence curve reflects the onset of deceleration of $\dot{\varepsilon}$, not the end of the phase of significant rifting. Thus, it is important to note that the onset of long-term subsidence in the constant force model is not necessarily equivalent to the end of active, significant, rifting.

3.2. Results of the strain hardening model (SHM)

3.2.1 Role of strain hardening parameters

The strain rate ($\dot{\varepsilon}$) as a function of time in the SHM is shown in Fig. 4, where the thickness of the thermal lithosphere (*a*) is 90 km, the initial thickness of the crust (t_c) is 30 km and the magnitude of tectonic force (F_a) is 4.9 TN/m. For the same F_a and crust/lithosphere thicknesses, the rifting process led to break-up in the model without strain hardening (RCM; see Fig. 3). However, the fate of rifting in the SHM is strongly dependent on the hardening parameters, as described below.

Fig. 4(a) shows $\dot{\varepsilon}$ as a function of time for different values of ε_o (strain required for the onset of hardening), where ΔE (the strain interval required for the completion of hardening) is 0.8 and δ (the factor controlling the increase in viscosity) is 100. For the model with $\varepsilon_o \leq 0.6$, $\dot{\varepsilon}$ initially increases with time and then decreases until the subsequent cessation of rifting. The deceleration of $\dot{\varepsilon}$ is initiated in a later phase for larger ε_o. On the other hand, when ε_o is more than 0.7 $\dot{\varepsilon}$ never

decelerates, as the onset of hardening is too late to prevent the acceleration of $\dot{\varepsilon}$.

Stress envelopes at various times for the SHM with $\varepsilon_o = 0.6$, $\delta = 100$, $\Delta E = 0.8$ and $F_a = 4.9$ TN/m are shown in Fig. 4(a). In order to demonstrate how the strain hardening works in the numerical model the stress envelope for the model without strain hardening is also depicted in the figure, in which the ductile stress is calculated using $\dot{\varepsilon}$ predicted by the SHM. The difference in mantle strength between the two models cannot be seen before t ~ 20 my, because finite strain is required for the onset of hardening. Subsequently, a significant increase in strength appears at t ~ 24 my in the SHM and $\dot{\varepsilon}$ begins to decelerate until the rifting terminates. Strengthening has progressed significantly by t ~ 30 my as the strain increases. However, mantle strength is no longer enhanced by strain hardening in later phases of rifting for one of two reasons: strain does not increase significantly for very low $\dot{\varepsilon}$ or strain hardening has been already completed.

Fig. 4 (b) shows the evolution of $\dot{\varepsilon}$ for various values of δ, where ε_o is 0.6 and ΔE is 0.8. $\dot{\varepsilon}$ accelerates to infinity for the model with $\delta \leq 25$. On the other hand, for the model with $\delta \geq 50$, $\dot{\varepsilon}$ initially increases with time and then begins to decrease around t ~ 24 my with rifting eventually ceasing. However, for the specific case of $\delta = 50$, the increase in viscosity is insufficient to stop rifting and $\dot{\varepsilon}$ re-accelerates immediately to infinity. It is also noted that Δt_D is evidently shorter for larger δ in the failure mode.

The influence of ΔE on the evolution of $\dot{\varepsilon}$ is depicted in Fig. 4(c), where ε_o is 0.6 and δ is 100. The deceleration of $\dot{\varepsilon}$ is initiated at time t ~ 24 my for any ΔE. However, $\dot{\varepsilon}$ accelerates again to infinity for $\Delta E \geq 0.9$ because the hardening process is too slow. In the rift failure mode Δt_D is clearly shorter for smaller ΔE.

3.2.2 The temporal evolutions of strain rate, stretching factor and tectonic subsidence for selected model parameters

Fig. 5 shows the temporal evolutions of $\dot{\varepsilon}$, β and ζ in the SHM with selected model parameters, where *a* and t_c are assumed to be 90 and 30 km, respectively. For the model with $\varepsilon_o = 0.4$, $\delta = 100$, $\Delta E = 0.7$ and $F_a = 5.8$ TN/m (see model I), $\dot{\varepsilon}$ begins to decelerate at t ~ 5 my. The onset of deceleration corresponds to the transition from an initial, rapid, subsidence phase to a subsequent, more subdued, long-term one. Since $\dot{\varepsilon}$ is not insignificant (i.e., $< 10^{-17}$ 1/s) for at least ~ 15 my after the onset of deceleration of $\dot{\varepsilon}$, the value β continues to increase after the initial, rapid, subsidence phase. Similar behaviour can be seen in the model with smaller F_a (see the model II). However, the onset of deceleration occurs later even though the same hardening parameters are adopted. This is because the strain reaches ε_o in a shorter time as $\dot{\varepsilon}$ is larger.

For the model with $\delta = 2$ (see model III), even though ε_o is smaller than in other models, the deceleration comes later than in the other models. This is because δ is not effective enough to respond immediately to the onset of the hardening process. In addition, although the onset of deceleration must correspond to the inflection point of subsidence, a clear transition from the rapid initial phase to the subsequent long-term phase is difficult to recognize.

3.2.3 The fate of rifting controlled by strain hardening parameters

As described above, the ultimate fate of rifting in the SHM is strongly controlled by the strain hardening parameters. Figs 6(a) and (b) show the maximum ΔE that results in the failure mode of rifting as a function of ε_o for the models with $t_c = 30$ and 40 km, respectively. Results are obtained for a model with $a = 90$ km and $F_{cu} < F_a \leq 6$ TN/m. Each line gives the boundary between the failure and break-up modes of rifting, above which termination of the rifting process is no longer possible. For example, for the model with $t_c = 30$ km, $\varepsilon_o = 0.4$ and $\delta = 10$, the rifting process leads to the failure mode for $\Delta E \leq 0.45$, but to the break-up mode for $\Delta E > 0.45$. Conditions of ε_o and ΔE for the failure mode are less sensitive as δ is larger.

If δ and ΔE are held constant, the upper limit of ε_o for the failure mode is higher for the model with $t_c = 40$ km than for the model with $t_c = 30$ km. In addition, when δ is more than 250 and more than 50 for the models with $t_c = 30$ and 40 km, respectively, the failure mode can be obtained for any ΔE. However, if ε_o exceeds 0.6 and 0.9 for the models with $t_c = 30$ and 40 km, respectively, the rifting process always results in the break-up mode for any ΔE, δ and F_a. The differences in the results between the models with $t_c = 30$ and 40 km indicate that replacement of crustal material with mantle material is an important factor in controlling the change in lithospheric strength. The replacement is larger for the model with greater t_c, so that the increase in lithospheric strength is larger for the model with $t_c = 40$ km.

The fate of rifting is also controlled by F_a, even in the SHM. The critical force (F_{cush}) in the SHM that results in the failure mode of rifting is summarized in Appendix B, showing the sensitivity of F_{cush} to the strain hardening parameters.

3.2.4 The onset of deceleration in the SHM

Fig 7 shows the time (t_d) when the deceleration of $\dot{\varepsilon}$ begins as a function of ε_o. Differences in δ are shown by different symbols. Results are shown only for the model with $a = 90$ km, where $\dot{\varepsilon}$ decreases to less than 10^{-17} (1/s) within 50 my. t_d is restricted to be less than ~ 30 and ~ 17 my for the models with $t_c = 30$ and 40 km, respectively. t_d, for given δ, ΔE and F_a, is, in general, greater for

greater ε_o. The dependence on ΔE can be seen for the model with relatively small δ; t_d is greater for greater ΔE. This is because the increase in viscosity is not sufficient to impose the deceleration of $\dot{\varepsilon}$ immediately. It is also noted that t_d is smaller for larger F_a because the strain ε_o for the onset of hardening is obtained in a shorter time interval for a larger $\dot{\varepsilon}$.

3.2.5 The duration of rifting in the SHM

Fig 8 summarizes the duration of rifting (Δt_D) as a function of δ for the model with a = 90 km and $F_{cu} < F_a \leq 6$ TN/m, where ε_o is held constant in each figure. Δt_D for a given δ has a wide range, depending on ΔE and F_a. However, the range of Δt_D becomes significantly narrower as ε_o increases. This is because the condition for the failure mode is narrower for larger ε_o. When ε_o has a critical value resulting in the failure mode of rifting, Δt_D is restricted to the ranges 24-38 my and 14-21 my for models with t_c = 30 and 40 km, respectively. The dependence of Δt_D on the model parameters is described in more detail in Appendix C, where it is shown that the relative importance of the assumed strain hardening mechanism with respect to hardening caused by thermal relaxation and crustal thinning should be taken into account in order to understand what controls Δt_D.

3.2.6 The stretching factor β in the SHM

Fig. 9 shows the stretching factor (β) achieved in the SHM with a = 90 km and $F_{cu} < F_a \leq 6$ TN/m. Only results obtained by models in which $\dot{\varepsilon}$ decreases to $< 10^{-17}$ (1/s) within 50 my are plotted. β displays a systematic dependence on ε_o and δ. β is generally greater for models with greater ε_o. In addition, β increases with δ when δ is smaller than ~ 10-100. However, when δ is greater than this, β decreases with an increase in δ. On the other hand, a systematic dependence on ΔE cannot be recognized. The sensitivities of β to the model parameters are described in more detail in Appendix D, where it is shown that the dependence of β on the strain hardening parameters is actually quite simple, except that the presence of an upper limit for each hardening parameter for the failure mode of rifting makes the results appear complicated.

The SHM reproduces a wide range of β, in which the maximum βs are up to ~ 3.5 and ~ 4.5 for the models with t_c = 30 and 40 km, respectively. It is also important to note that βs are generally larger for models with t_c = 40 km than for models with t_c = 30 km. This implies that crustal thinning plays an important role in controlling β even in the SHM. Strengthening by crustal thinning is greater for the model with t_c = 40 km, so that the failure mode of rifting can be still obtained even for the model with greater values of ε_o and ΔE.

4. Discussion

4.1 Tectonic subsidence in the constant force model

In this study, it is found that a deceleration of $\dot{\varepsilon}$ corresponds to an inflection point of the subsidence curve in the constant force model. This inflection point has been usually regarded as the transitional from syn- to post-rift subsidence. However, crustal thinning in the model still continues for some time even after the end of "syn-rift" like subsidence and, accordingly, the "post-rift" like subsidence is brought about not only by thermal relaxation but also by crustal thinning (see Figs 3 and 5). Therefore, if the observed stretching factor is applied to the simple pure shear stretching model, the amount of initial subsidence is overestimated, while that of subsequent long-term subsidence is underestimated.

It is well known that the initial and subsequent long-term magnitudes of subsidence observed in sedimentary basins are often, respectively, smaller and larger than that predicted by simple stretching model. This feature of subsidence has been found in sedimentary basins not only where the rifting led to seafloor spreading (e.g., Royden and Keen, 1980; Beaumont et al., 1982) but also where the rifting did not lead to break-up (e.g., Torres et al., 1993; Sclater and Christie, 1980; Sclater et al., 1980; Royden et al., 1983; Artyushkov, 1992; Spadini et al., 1997; Skogseid, 2000). Several models have been proposed to explain the contradiction, including depth-dependent stretching (e.g., Royden and Keen, 1980), emplacement of magma (e.g., Sclater et al., 1980; White and McKenzie, 1989), phase transitions in the crust and/or mantle (e.g., Arthyushkov, 1992; Podladchikov et al., 1994; Yamasaki and Nakada, 1997; Petrini et al., 2001; Kaus et al., 2005) and lateral lower crustal flow from rift centre to adjacent areas induced by sediment loading and erosional unloading (Morley and Westaway, 2006). However, as described above, such a commonly observed feature of subsidence is actually consistent with the configuration of the constant force model. The contradiction is caused by an overestimation of initial subsidence and an underestimation of long-term subsidence without considering that the ultimate stretching factor is not obtained at the end of "syn-rift" like subsidence phase.

4.2 Stretching factors and rift duration in the reference conventional model (RCM)

For rifts that fail ("failure mode") in the RCM, maximum stretching factors (β) are generally quite small compared to some reported values. It has been shown that, when the thickness of the thermal lithosphere (a) is 90 km, it is impossible to obtain β more than 1.55 and 1.60 for models with t_c (the initial thickness of the crust) of 30 and 40 km, respectively. Based on models with other as, it has also been confirmed that β in the RCM is less than 1.85. β inferred in many sedimentary basins is generally less than 2.0 (e.g., Newman and White, 1997). However, it is still necessary to explain β

greater than 2.0 as observed in real rift systems such as, for example, the Valencia Trough ($\beta > 3.0$; Torres et al., 1993), the Pannonian Basin ($\beta \sim 3.0$; e.g., Sclater et al., 1980; Royden et al., 1983), the Aegean Sea ($\beta \sim 2.0$; Makris, 1975; Makris and Vees, 1977), and the Rockall Trough ($\beta \sim 5.0$; Makris et al., 1991; Keser Neish, 1993; Shannon et al., 1993; O'Reilly et al., 1995; Skogseid et al., 2000).

Another issue with the RCM relates to the duration of the rifting process (Δt_D). Many sedimentary basins have developed with active rifting terminating in less than 20 ~ 30 my (e.g., Jarvis and McKenzie, 1980; Allen and Allen, 2005). However, it is shown here that the RCM with a = 90 km cannot predict Δt_D less than 40 ~ 50 my (see Figs 3(a) and (b)). For the model with greater a, additionally, Δt_D must be longer because the characteristic time-scale of thermal relaxation is a function of a. One reason why the RCM predicts rift durations longer than often reported is because of the definition used to define the cessation of rifting. Usually, the duration of rifting is based on the inflection point taken to define the transition from "syn-rift" to "post-rift" like subsidence, whereas it was based on the strain rate dropping to less than 10^{-17} (1/s) above. In this study we have shown that the inflection point can occur at times slightly less than ~ 20 my (see Figs 3(a) and (b)). Nevertheless, the model that predicts such a short duration of the "syn-rift" like subsidence has difficulty in explaining a significant amount extension, especially when the thickness of the crust is relatively thin (t_c = 30 km). Additionally, the deceleration of the rifting process, especially for the model with a thinner initial crust (t_c = 30 km), is not strong enough to reproduce a clear transition from "syn-rift" like to "post-rift" like subsidence that is a general characteristic feature of most rift-related sedimentary basins (McKenzie, 1978).

The RCM can indeed predict a larger β-factor by considering a more numerically precise magnitude of tectonic force: for example, β-factor inferred from the model with a = 90 km, t_c = 40km and F_a = 1.456 TN/m is 3.06. However, it is still difficult for the model with such a precise magnitude of tectonic force to explain the observed range of rift durations (or initial subsidence phase).

Thus, it is difficult for the RCM to explain a significant amount of extension achieved in a short duration of rifting (or "syn-rift" like subsidence). Even though rifting must be initiated with a significantly large strain rate in order to obtain large stretching factors observed in sedimentary basin, strengthening by thermal relaxation and crustal thinning has no potential to stop such a rifting process. Additionally, even for a magnitude of tectonic force that results in the failure mode, strengthening by these two factors is still not enough to produce the apparent transition between the two subsidence phases. The results of the RCM imply that it is required to introduce some additional hardening mechanism to resolve these limitations vis-à-vis the observational dataset.

4.3 Role of strain hardening

The SHM is better than the RCM in explaining a wide variety of observed features. In the SHM, the duration of the initial, rapid, subsidence phase that ends with the onset of deceleration of $\dot{\varepsilon}$ is predicted to be less than ~ 30 my, depending on the hardening parameters and F_a ($> F_{cu}$) (see Fig. 7). Therefore, whatever the physical mechanism is, the presence of significant hardening allows us to predict the duration of the "syn-rift" like subsidence phase observed in many sedimentary basins. The longer duration of the initial subsidence phase may be attributed to the absence of hardening or a lower magnitude of F_a ($\leq F_{cu}$). On the other hand, the dependence of Δt_D (the duration of actual rifting) on the model parameters is more complicated, because the effects of crustal thinning and thermal relaxation should also be taken into account (see Appendix C). For this reason, however, a wide range of actual rifting durations can be obtained, including those from observed data (see Fig. 8), by adjusting the hardening parameters and F_a. In addition, the SHM also has the potential to reproduce significantly greater β-factors than the RCM (see Fig. 9).

Although it is important to apply the SHM to real sedimentary basins to assess its potential, realistic values of the strain hardening parameters have not been evaluated in the present study. Since an actual, realistic, hardening mechanism has not been specified, it is irrelevant to discuss exact values of each hardening parameter. However, hardening parameters that satisfy observations may offer some insight into possible hardening mechanisms. Here, as a first step, sensitivities of model behaviour to the strain hardening parameters have been investigated on the grounds that this should be helpful in surmising any appropriate hardening mechanism that might contribute to explaining observed features of real sedimentary basins. Further investigations along these lines may be a fruitful future endeavour.

4.4 Strain hardening mechanism: implications for the fate of rifting

The adopted strain hardening formula is not based on a specific physical mechanism and, as such, is applicable to any possible hardening phenomenon. One possible mechanism might be work hardening caused by dislocation multiplication. Chopra and Paterson (1981) reported that stress increments on the order of a few hundred MPa for a few % of strain is required to maintain a constant strain rate and, based on this, Hobbs and Ord (1988) investigated the role of strain hardening in the occurrence of plastic instabilities in subducting slabs as a mechanism of deep focus earthquakes. However, a strain less than 10 % corresponds to a stretching factor less than 1.1. If hardening takes place at such small strain, a significantly larger stretching factors, like those observed in real sedimentary basins, would be difficult to obtain. A more serious problem is that the effect of work

hardening might be reduced or even eliminated by dynamic recrystallization as deformation progresses, resulting in strain softening (e.g., Karato et al., 1980; Tullis and Yund, 1985; Hirth and Tullis, 1992).

Another potential candidate, for which there exists some observational and experimental evidence, could be a switch from wet to dry rheology during rifting (The term "strain hardening" may not be strictly appropriate for this mechanism. However, as described below, the "hardening" does possibly take place as strain increases and the term is applied in this sense.) Based on the higher solubility of water in basaltic magma than in olivine (e.g., Burnham, 1979; Mackwell et al., 1985), Karato (1986) suggested that partial melting could cause an increase in viscosity as long as only a small melt fraction remains in the parent rock. Later, Hirth and Kohlstedt (1996) examined this hypothesis quantitatively, showing that water is efficiently extracted by adiabatic decompressional melting at depths of between 120 and 65 km beneath mid-ocean ridges and that the viscosity can be increased by a factor ~1000 (from 10^{18} to 10^{21} Pa s). This range of viscosity increase is large enough to terminate rifting (see Fig. 6).

Previous numerical studies (e.g., McKenzie and Bickle, 1988; White and McKenzie, 1989; Harry et al., 1993; Harry and Leeman, 1995) showed that the amount of melt produced during extension depends strongly on β and a as well as the asthenospheric potential temperature (T_a). If a and T_a are held constant, the amount of melt increases as β increases. Additionally, melting is suppressed until some minimum degree of lithospheric thinning occurs. Therefore, melting-induced dehydration of the lithosphere can be considered to start after some critical strain is achieved and occurs thereafter progressively over a finite amount of extension. These characteristics are simulated by the strain hardening model implemented here.

The melting process should be influenced by the temporal change in temperature and pressure of each material point (e.g., McKenzie, 1984), so that $\dot{\varepsilon}$ must be an important factor in controlling the melting process. In addition, as can be seen in Hirth and Kohlstedt (1996), the initial water content in the mantle peridotite is also an important factor. Therefore, a wide variety of possible strain hardening mechanisms (i.e., represented in the present model by a wide variety of hardening parameter combinations) may be necessary to emulate such complex dependencies in the melting process. Indeed, sedimentary basin development and associated magmatic activity shows in general strong regional differences (e.g., Ziegler and Cloetingh, 2004).

From the viewpoint of a melting-induced hardening hypothesis, a large volume generated melt must favour the hardening process. However, the decrease in viscosity due to the presence of melt may counteract the increase in viscosity due to the extraction of water (e.g., Kohlstedt and Zimmerman, 1996). Although the upward migration of melt can be an additional hardening mechanism by

enhancing the effective thermal diffusivity (Takeshita and Yamaji, 1990), continental break-up is usually accompanied by intense magmatic activity. Many studies have emphasized the importance of magmatism as the possible origin of strain localization in controlling continental break-up (e.g., Ebinger and Casey, 2001; Gernigon et al., 2004; Geoffroy, 2005; Ebbing et al., 2006; Ranalli et al., 2007). Even at non-volcanic passive margins, it is difficult to avoid producing melts in the rifting process (e.g., Pérez-Gussinyé et al., 2006) and the break-up process is generally discussed in the context of magmatic activity (e.g., Tucholke et al., 2007). These kinds of considerations – that melt generation is closely associated with continental break-up – imply that it is at least to some degree problematic to consider the generation of melts in the present model as a significant source of strain hardening. The competition between the hardening and softening processes associated with the generation of the melts remains as matter of further quantitative investigation.

It is also noted that analogue and numerical modelling studies (Corti et al., 2007; Yamasaki and Gernigon, 2007) have shown that, because deformation may otherwise be distributed over a broad region, a narrow rheological heterogeneity is favourable for obtaining strain localization. Thus, as pointed out by Yamasaki and Gernigon (2007), the emplacement of a large volume of magmatic rocks prior to the onset of continental break-up may inhibit the formation of a localized break-up point. The implication of this is that the break-up process would have to be initiated in the presence of only a small amount of melt such that melt-induced dehydration and strain hardening would not yet be capable of decelerating the rifting process. It follows, in terms of the implications of the present model, that the "fate" of rifting – that it will be the break-up mode – has already been decided prior to voluminous magmatism such as typically associated with the break-up process.

That is to say, even if significant hardening is imposed by voluminous magmatic activity, the rifting process remains difficult to be terminated when the magnitude of tectonic force is greater than some critical value, which, in turn, can be strongly dependent on the relevant hardening process. On the other hand, even if significant hardening is not achieved by melt-related dehydration (or any other mechanism), rifting could still be terminated when the magnitude of tectonic force is less than the critical value. Therefore, the fate of rifting is primarily controlled by the magnitude of tectonic force: whether break-up or failure occurs, it is the end product of a process that is initiated with a given F_a that is either greater than or less than some critical value that is dependent on other physical parameters. However, the effect of "strain hardening" induced by melt-induced dehydration may become important when the extensional tectonic force is less than its critical value in the first place.

5. Concluding remarks

The rheology-controlled cessation of rifting has been discussed on the basis of a simple one-dimensional constant force model with strain hardening. Most of the considerations discussed above lead to the idea that the magnitude of force is the dominant factor that determines whether rifting fails or leads to continental break-up, even in the presence of significant strain hardening. In the failure mode of rifting, however, the style of rifting is strongly controlled by the strain hardening parameters.

Depending on parameters that define the hardening process, the model explains a wider range of features observed in many failed-rift sedimentary basins than a conventional model without strain hardening. A detailed analysis of how the results depend on the adopted hardening parameters has allowed some constraint to be placed on what the actual physical mechanism of strain hardening might be. One possible hardening mechanism that is consistent with what can be inferred from the model results is the extraction of water associated with decompressional melting during rifting. In this case, a variety of different rifting styles may be explicable in terms of a partial melting process that is controlled by the initial thermal conditions of the lithosphere and asthenosphere, the extensional strain rate (i.e. applied tectonic force) and the initial water content of the mantle.

The results also suggest some important insights into the behaviour of basin subsidence in relation to the dynamics of rifting. The transition from initial, rapid, "syn-rift" like subsidence to a more passive "post-rift" like subsidence corresponds to a deceleration of rifting rate rather than the complete cessation of extensional strain. As such, the model implies that syn- and post-rift subsidence magnitudes are, respectively, overestimated and underestimated if interpreted in terms of a simple, conventional, stretching model.

It has been in practice difficult to evaluate whether the rifting process is controlled dominantly by temporal changes in the magnitude of tectonic forces or by rheological changes in the lithosphere, intrinsic to the rifting itself. This is because observable features of sedimentary basin formation can be explained by either rheology- or force-controlled hypotheses. Newman and White (1999) argued against a force-controlled rifting process; nevertheless, it obviously cannot be ruled out that rapid changes in tectonic force levels (and orientations) may be responsible for a particular lithospheric structural evolution (e.g. Nielsen et al., 2007). In order to test the hypothesis of rheology-controlled cessation of rifting, as proposed here, realistic strain hardening mechanisms and the parameters that define them obviously require additional quantitative investigation.

Acknowledgements

We would like to thank Satoru Honda, Hikaru Iwamori and Yoshitaka Takeda for many fruitful discussions and helpful suggestions. Constructive reviews of Giorgio Ranalli and Wolf Jacoby have

significantly improved the manuscript. Jean Braun, Scott King and anonymous reviewers are also acknowledged for constructive and critical reviews of earlier versions. The calculations in this study were carried out on the computer facilities at the Dublin Institute for Advanced Studies and University College Dublin. This study was partly supported by the CosmoGrid Project, which is funded by the Program for Research in Third Level Institutions under the Irish National Development Plan and with assistance from the European Regional Development Fund, and carried out as part of the WestMed project of the European Science Foundation EUROMARGINS programme.

Appendix A. The critical tectonic force in the reference conventional model (RCM)

When the magnitude of tectonic force (F_a) is beyond the upper critical value (F_{cu}), the rifting process cannot be terminated. On the other hand, when F_a is less than the lower critical value (F_{cl}), the strain rate ($\dot{\varepsilon}$) is too small (less than 10^{-17} (1/s)) to obtain a significant extension of the lithosphere. Fig. A summarizes F_{cu} and F_{cl} as a function of the thickness of the thermal lithosphere (a) for different crustal thicknesses (t_c). F_{cu} and F_{lc} are greater for greater a and smaller for greater t_c because of the temperature dependence of the viscosity and the intrinsically weaker crust than the mantle. F_{cu} with t_c = 30 and 40 km is less than the currently accepted maximum magnitude of tectonic force (~ 6 TN/m) for the models with $a \leq 95$ km and $a \leq 130$ km, respectively, implying that such a crust-lithosphere configuration can be in effect unstable for the RCM. F_{cl} with t_c = 30 and 40 km is predicted to be less than ~ 6 TN/m for the models with $a \leq 105$ km and $a < 150$ km, respectively, meaning that no rifting would take place for these crust-lithosphere model configurations.

Appendix B. The critical tectonic force in the strain hardening model (SHM)

Fig. B shows the maximum ΔE (the strain interval required for the completion of hardening) resulting in the failure mode as a function of F_a for different δs (the factor controlling the increase in viscosity), where ε_o (the strain required for the onset of hardening) is held constant in each figure. Black and gray curves represent the models with t_c = 30 and 40 km, respectively. Results are obtained by the model with a = 90 km and $F_{cu} < F_a \leq 6$ TN/m, and the upper critical tectonic force (F_{cu}) in the RCM is indicated by vertical dotted lines. It is evidently true that the rifting process is always convergent in the SHM with $F_a \leq F_{cu}$.

The conditions of ε_o and ΔE for the failure mode become wider as δ increases, but no hardening process can terminate the rifting process with $F_a > F_{cu}$ if ε_o is more than the critical value. The critical tectonic force (F_{cush}) in the SHM strongly depends on the hardening parameters, in which F_{cush} is larger for smaller ε_o, larger δ and smaller ΔE. It is also noted that F_{cush} is smaller for the model with t_c = 40

km than for the model with t_c = 30km. Even though the model with larger t_c is more favourable for obtaining an increase in lithospheric strength, the condition for the failure mode with t_c = 40 km is rather narrower in the range of reasonable magnitudes of tectonic force ($F_a \leq 6$ TN/m).

Appendix C. Factors controlling the duration of rifting (Δt_D)

Fig. C (a) shows Δt_D as a function of δ for the model with t_c = 30 km in order to examine its dependence on ΔE and F_a, for three models with F_a = 4.9, 5.5 and 6.0 TN/m and ε_o is 0.0. It can be seen that Δt_D decreases with δ and increases with ΔE for relatively large δ; it is clear that, once the deceleration of $\dot{\varepsilon}$ takes place, the subsequent duration of rifting must be shorter for larger δ and smaller ΔE.

On the other hand, Δt_D increases with δ but decreases with ΔE for relatively small δ, which can be seen more clearly for larger F_a. This behaviour may be related to the fact that t_d (the time when the deceleration of $\dot{\varepsilon}$ begins) is dependent on ΔE for relatively small δ. However, similar behaviour is also seen for the model in which δ is large enough not to show the dependence of t_d on ΔE. That is, even though the onset of deceleration occurs at the same time, Δt_D is predicted to be shorter for larger ΔE and smaller δ. Smaller Δt_D for smaller δ and larger ΔE is predicted only when ε_o is less than 0.1. Similar behaviour can be seen more clearly for the model with t_c = 40 km (see Fig. D(b)), in which the smaller Δt_D for smaller δ and larger ΔE is predicted only when ε_o is less than 0.4.

The model behaviour of Δt_D is a matter of whether strengthening by crustal thinning and thermal relaxation works dominantly on the deceleration of rifting or not. As can be seen in Fig.3, strengthening by these two factors works more effectively for a higher $\dot{\varepsilon}$, which also explains why Δt_D is predicted to be shorter for larger ΔE. The deceleration takes place more slowly for smaller δ and larger ΔE, so that $\dot{\varepsilon}$ stays high enough for a longer period to make the strengthening by crustal thinning and thermal relaxation more significant. This results in an enhancement of deceleration at a later phase. For the model with sufficiently large δ the deceleration of rifting takes place soon enough thereafter such that Δt_D is mainly controlled by the imposed strain hardening. Thus, when Δt_D as a function of δ has a positive slope (i.e. Δt_D increases as δ increases), strengthening by crustal thinning and thermal relaxation plays the dominant role in decelerating rifting. On the other hand, when Δt_D as a function of δ has a negative slope (i.e. Δt_D decreases as δ increases), the strain hardening effect is dominant.

The dependence of Δt_D on F_a can also be explained in terms of the relative importance of strain hardening to strengthening by crustal thinning and thermal relaxation. Δt_D is predicted to be smaller for larger F_a under the condition that Δt_D as a function of δ has a positive slope. The strain hardening

process can be completed more readily for a higher $\dot{\varepsilon}$ resulting from a larger F_a, which is also another possible mechanism to explain a smaller Δt_D for larger F_a. However, it is difficult for this mechanism to explain the positive slope of the Δt_D curve as a function of δ. On the other hand, Δt_D is predicted to be larger for larger F_a under the condition that Δt_D as a function of δ has a negative slope. This is because a greater time interval is required to terminate the rifting process that is taking place with higher $\dot{\varepsilon}$.

Appendix D. Sensitivity of stretching factor to model parameters

Fig. D(a) shows the dependence of β on ε_o for models with t_c = 30 and 40 km, with *a* being 90 km and F_a and δ held constant. The lowest value of ΔE is 0.0. The upper limit of ΔE for a given ε_o, resulting in the failed rift mode, can be read from in the figures. β for a given ΔE is larger for larger ε_o. In addition, β for a given ε_o is larger for ΔE. The maximum β for given F_a, ε_o and δ is obtained by the model with the critical value of ΔE, but the critical value of ε_o does not always give the maximum β for given F_a and δ.

Fig. D(b) shows the dependence of β on δ for models with t_c = 30 and 40 km, with *a* being 90 km and F_a and ε_o held constant. β for a given ΔE is larger for smaller δ. Since it becomes more difficult for smaller δ and larger ΔE to obtain the failure mode of rifting, β for δ = 10 can be larger than that for δ = 5 in the model with t_c = 30 km.

Fig. D(c) shows the dependence of β on F_a for models with t_c = 30 and 40 km, with *a* being 90 km and ε_o and δ held constant. β for a given ΔE is larger for larger F_a. It should be noted that a larger β is not always obtained by the model with a larger F_a because there are other critical parameter values for obtaining the failure mode of rifting.

References

Allen, P.A., Allen, J.R., 2005. Basin Analysis, Second ed., Blackwell Publishing Ltd, pp. 549.

Artyushkov, E.V., 1992. Role of crustal stretching on subsidence of the continental crust. Tectonophysics 215, 187-207.

Bassi, G., 1991. Factors controlling the style of continental rifting: insights from numerical modelling. Earth Planet. Sci. Lett. 105, 430-452.

Bassi, G., 1995. Relative importance of strain rate and rheology for the mode of continental extension. Geophys. J. Int. 122, 195-210.

Beaumont, C., Keen, C., Boutilier, R., 1982. On the evolution of rifted continental margins: comparison of models and observations for the Nova Scotia margin. Geophys. J. R. Astron. Soc. 70, 667-715.

Bott, M.H.P., 1982. Origin of lithospheric tension causing basin formation. Philos, Trans. R. Soc. London., 305, 319-324.

Bott, M.H.P., 1991. Ridge push and associated plate interior stress in normal and hot spot regions. Tectonophysics 200, 17-32.

Bott, M.H.P., Waghorn, G.D., Whittaker, A., 1989. Plate boundary forces at subduction zones and trench-arc compression. Tectonophysics 170, 1-15.

Brace, W.F., Kohlstedt, D.L., 1980. Limits on lithospheric stress imposed by laboratory experiments. J. Geophys. Res. 85, 6248-6252.

Braun, J., Beaumont, C., 1987. Styles of continental rifting: Results from dynamic models of lithospheric extension. Can. Soc. Pet. Geol. Mem. 12, 241-258.

Braun, J., Beaumont, C., 1989. Dynamic models of the role of crustal shear zones in asymmetric continental extension. Earth Planet. Sci. Lett. 93, 405-423.

Buck, W.R., 1991. Modes of continental lithospheric extension. J. Geophys. Res. 96, 20,161-20,178.

Burnham, C.W., 1979. The importance of volatile constituents, in: Yoder Jr., J.S. (Eds.), The evolution of the igneous rocks, Princeton Univ. Press, 439-482.

Byerlee, J.D., 1978. Friction of rocks. Pure Appl. Geophys. 116, 615-626.

Carter N.L., Tsenn, M.C., 1987. Flow properties of continental lithosphere. Tectonophysics 136 27-63.

Chopra, P.N., Paterson, M.S., 1981. The experimental deformation of Dunite. Tectonophysics 78 453-473.

Corti, G., Bonini, M., Innocenti, F., Manetti, P., Piccardo, G.B., Ranalli, G., 2007. Experimental models of extension of continental lithosphere weakened by percolation of asthenospheric melts. J. Geodyn. 43 465-483.

Corti, G., Manetti, P., 2006. Asymmetric rifts due to asymmetric Mohos: An experimental approach. Earth Planet. Sci. Lett. 245, 315-329.

Dunbar, J.A., Sawyer, D.S., 1988. Continental rifting at pre-existing lithospheric weaknesses. Nature 333 450-452.

Ebbing, J., Lundin, E., Olesen, O., Hansen, E.K., 2006. The mid-Norwegian margin: a discussion of crustal lineaments, mafic intrusions and remnants of the Caledonian root by 3D density modelling and structural interpretation. J. Geol. Soc. Lond. 163 47-59.

Ebinger, C. J., Casey, M., 2001. Continental breakup in magmatic provinces: An Ethiopian example. Geology 29, 527-530.

England, P., 1983. Constraints on extension of continental lithosphere. J. Geophys. Res. 88, 1145-1152.

Ershov, A.V., Stephenson, R.A., 2006. Implications of a visco-elastic model of the lithosphere for

calculating yield strength envelopes. J. Geodyn., 42, 12-27.

Fernàndez, M., Ranalli, G., 1997. The role of rheology in extensional basin formation modelling. Tectonophysics 282, 129-145.

Forsyth, D., Uyeda, S., 1975. On the relative importance of the driving forces of plate motion. Geophys. J. R. Astron. Soc. 43, 163-200.

Frederiksen, S., Braun, J., 2001. Numerical modelling of strain localization during extension of the continental lithosphere. Earth Planet. Sci. Lett. 188, 241-251.

Geoffroy, L., 2005. Volcanic passive margin. Comptes Rendus Geosciences 337 1395-1408.

Gernigon, L., Ringenbach, J.-C., Planke, S., Le Gall, B., 2004. Deep structures and breakup along volcanic rifted margins: insights from integrated studies along the outer Vøring Basin (Norway). Mar. Petro. Geol. 21 363-372.

Goetze, C., Evans, B., 1979. Stress and temperature in the bending lithosphere as constrained by experimental rock mechanics. Geophys. J. R. astr. Soc. 59, 463-478.

Govers, R., Wortel, M.J.R., 1993. Initiation of asymmetric extension in continental lithosphere. Tectonophysics 223, 75-96.

Govers, R., Wortel, M.J.R., 1995. Extension of stable continental lithosphere and the initiation of lithospheric scale faults. Tectonics 14, 1041-1055.

Harry, D.L., Leeman, W.P., 1995. Partial melting of melt metasomatized subcontinental mantle and the magma source potential of the lower lithosphere. J. Geophys. Res. 100, 10,255-10269.

Harry, D.L., Sawyer, D.S., Leeman, W.P., 1993. The mechanics of continental extension in western North America: implications for the magmatic and structural evolution of the Great Basin. Earth Planet. Sci. Lett. 117, 59-71.

Hirth, G., Kohlstedt, D.L., 1996. Water in the oceanic upper mantle: implications for rheology, melt extraction and the evolution of the lithosphere Earth Planet. Sci. Lett. 144, 93-108.

Hirth, G., Tullis, J., 1992. Dislocation creep regimes in quartz aggregates. J. struct. Geol. 14 145-159.

Hobbs, B.E., Ord, A., 1988. Plastic instabilities: implications for the origin of intermediate and deep focus earthquakes. J. Geophys. Res. 93 10,521-10,540.

Hopper, J.R., Buck, W.R., 1993. The initiation of rifting at constant tectonic force: Role of diffusion creep. J. Geophys. Res. 98, 16,213-16,221.

Huismans, R.S., Beaumont, C., 2002. Asymmetric lithospheric extension: The role of frictional plastic strain softening inferred from numerical experiments. Geology 30, 211-214.

Huismans, R.S., Beaumont, C., 2003. Symmetric and asymmetric lithospheric extension: Relative effects of frictional-plastic and viscous strain softening. J. Geophys. Res. 108, 2496,

doi:10.1029/2002JB002026.

Jarvis, G.T., McKenzie, D.P., 1980. Sedimentary basin formation with finite extension rates. Earth Planet. Sci. Lett., 48, 42-52.

Karato, S., 1986. Does partial melting reduce the creep strength of the upper mantle? Nature 319, 309-310.

Karato, S., Paterson, M.S., Fitz Gerald, J.D., 1986. Rheology of synthetic olivine aggregates: Influence of grain size and water. J. Geophys. Res. 91, 8151-8176.

Karato, S., Toriumi, M., Fujii, T., 1980. Dynamic recrystallization of olivine single crystals during high-temperature creep. Geophys. Res. Lett. 7 649-652.

Kaus, B.J.P., Connolly, J.A.D., Podladchikov, Y.Y., Schmalholz, S.M., 2005. Effect of mineral phase transitions on sedimentary basin subsidence and uplift. Earth Planet. Sci. Lett. 233, 213-228.

Keser Neish, J., 1993. Seismic structure of the Hatton-Rockall area: an integrated seismic/modelling study from composite data sets, in: Parker, J.R. (Eds.), Petroleum Geology of Northwest Europe: Proceedings of the 4th Conference, Geol. Soc. Lond. 1047-1056.

Koch, P.S., Christie, J.M., Ord, A., George, Jr., R.P., 1989. Effect of water on the rheology of experimentally deformed quartzite. J. Geophys. Res. 94, 13,975-13,996.

Kohlstedt, D.L., Evans, B., Mackwell, S.J., 1995. Strength of the lithosphere: Constraints imposed by laboratory experiments. J. Geophys. Res. 100, 17,587-17,602.

Kohlstedt, D.L., Zimmerman, M.E., 1996. Rheology of partially molten mantle rocks. Annu. Rev. Earth Planet. Sci. 24, 41-62.

Kusznir, N.J., 1982. Lithosphere response to externally and internally derived stresses: a viscoelastic stress guide with amplification. Geophys. J. R. astr. Soc., 70, 399-414.

Kusznir, N.J., Park, R.G., 1987. The extensional strength of the continental lithosphere: its dependence on geothermal gradient, and crustal composition and thickness, in: Coward, M.P., Dewey, J.F., Hancock, P.L. (Eds.), Continental Extensional Tectonics, Geol. Soc. Spec. Pub. 28, 35-52.

Le Pichon, X., 1983. Land-locked oceanic basins and continental collision: the Eastern Mediterranean as a case example. In: Hsu, K.J. (Eds.), Mountain Building Process, pp. 201-211, Academic Press.

MackWell, S.J., Kohlstedt, D.L., Paterson, M., 1985. The role of water in the deformation of olivine single crystals. J. Geophys. Res. 90, 11,319-11,333.

Makris, J., 1975. Crustal structure of the Aegean Sea and the Hellenides obtained from geophysical surveys. J. Geophys. 41, 441-443.

Makris, J., Ginzburg, A., Shannon, P.M., Jacob, A.W.B., Bean, C.J., Vogt, U., 1991. A new look at the Rockall region, offshore Ireland. Mar. Petro. Geol. 8, 410-416.

Makris, J., Vees, R., 1977. Crustal structure of the central Aegean Sea and the islands of Evia and Crete, Greece, Obtained by refraction seismic experiments. J. Geophys. 42, 329-341.

Martinez, F., Cochran, J.R., 1988. Structure and tectonics of the northern Red Sea: catching a continental margin between rifting and drifting. Tectonophysics 150, 1-31.

McKenzie, D.P., 1978. Some remarks on the development of sedimentary basins. Earth Planet. Sci. Lett. 40, 25-32.

McKenzie, D., 1984. The generation and compaction of partially molten rock. J. Ptrol. 25, 713-765.

McKenzie, D., Bickle, J.M., 1988. The volume and composition of melt generated by extension of the lithosphere. J. Petrol. 29, 625-679.

Morley, C. K., Westaway, R., 2006. Subsidence in the super-deep Pattani and Malay basins of Southeast Asia: a coupled model incorporating lower-crustal flow in response to post-rift sediment loading. Basin Res. 18, 51-84.

Negredo, A.M., Fernàndez, M., Zeyen, H., 1995. Thermo-mechanical constraints on kinematic models of lithospheric extension. Earth Planet. Sci. Lett. 134, 87-98.

Newman, R., White, N., 1997. Rheology of the continental lithosphere inferred from sedimentary basins. Nature 385, 621-624.

Newman, R., White, N., 1999. The dynamics of extensional sedimentary basins: constraints from subsidence inversion. Phil. Trans. R. Soc. Lond. A357, 805-834.

Nielsen, S.B., Stephenson, R., Thomsen, E., 2007. Dynamics of Mid-Palaeocene North Atlantic rifting linked with European intra-plate deformations. Nature 450, 1071-1074.

O'Reilly, B.M., Hauser, F., Jacob, A.W.B., Shannon, P.M., Makris, J., Vogt, U., 1995. The transition between the Erris and the Rockall basins: new evidence from wide angle seismic data. Tectonophysics 241, 143-163.

Parsons, B., Richter, F.M., 1980. A relation between the driving force and geoid anomaly associated with mid-ocean ridges. Earth Planet. Sci. Lett. 51 445-450.

Petrini, K., Connolly, J.A.D., Podladchikov, Y.Y., 2001. A coupled petrological – tectonic model for sedimentary basin evolution: the influence of metamorphic reactions on basin subsidence. Terra Nova 13, 354-359.

Pérez-Gussinyé, M., Phipps Morgan, J., Reston, T.J., Ranero, C.R., 2006. The rift to drift transition at non-volcanic margins: Insights from numerical modelling. Earth Planet. Sci. Lett. 244, 458-473.

Podladchikov, Y.Y., Poliakov, A.N.B., Yuen, D.A., 1994. The effect of lithospheric phase transitions on subsidence of extending continental lithosphere. Earth Planet. Sci. Lett. 124, 95-103.

Ranalli, G., 1995. Rheology of the Earth, Second ed., Chapman and Hall, pp. 413.

Ranalli, G., Piccardo, G.B., Corona-Chavez, P., 2007. Softening of the subcontinental lithospheric mantle by asthenosphere melts and the continental extension/oceanic spreading transition. J. Geodyn. 43 450-464.

Royden, L., Horvath, F., Nagymarosy, A., Stegena, L., 1983. Evolution of the Pannonian basin system 2. subsidence and thermal history. Tectonics 2, 91-137.

Royden, L., Keen, C.E., 1980. Rifting process and thermal evolution of the continental margin of eastern Canada determined from subsidence curves. Earth Planet. Sci. Lett. 51, 343-361.

Schellart, W.P., 2004. Quantifying the net slab pull force as a driving mechanism for plate tectonics. Geophys. Res. Lett. 31 L07611 doi: 10.1029/2004GL019528.

Sclater, J.G., Christie, P.A.F., 1980. Continental stretching: an explanation for the post-Mid-Cretaceous subsidence of the central North Sea Basin. J. Geophys. Res. 85, 3711-3739.

Sclater, J.G., Royden, L., Horvath, F., Burchfiel, B.C., Semken, S., Stegena, L., 1980. The formation of the intra-Carpathian basins as determined from subsidence data. Earth Planet. Sci. Lett. 51, 139-162.

Shannon, P.M., Moore, J.G., Jacob, A.W.B., Makris, J., 1993. Cretaceous and Tertiary basin development west of Ireland, in: Parker, J.R. (Eds.), Petroleum Geology of Northwest Europe: Proceedings of the 4th Conference, Geol. Soc. Lond. 1057-1066.

Shelton, G., Tullis, J., 1981. Experimental flow laws for crustal rocks. EOS 62, 396.

Skogseid, J., Planke, S., Faleide, J.I., Pedersen, T., Eldholm, O., Neverdal, F., 2000. NE Atlantic continental rifting and volcanic margin formation, in: Nottvedt, A. (Eds.), Dynamics of the Norwegian Margin, Geol. Soc. Spec. Pub. 167, 295-326.

Spadini, G., Robinson, A., Cloetingh, S., 1997. Thermo-mechanical modelling of Black Sea formation, subsidence and sedimentation, in: Robinson, A. (Eds.), Regional and Petroleum Geology of the Black Sea and Surrounding Areas. AAPG Mem. 68, 19-38.

Takeshita, T., Yamaji, A., 1990. Acceleration of continental rifting due to a thermomechanical instability. Tectonophysics 181, 307-320.

Torres, J., Bois, C., Burrus, J., 1993. Initiation and evolution of the Valencia Trough (western Mediterranean): constraints from deep seismic profiling and subsidence analysis. Tectonophysics 228, 57-80.

Tucholke, B.E., Sawyer, D.S., Sibuet, J.-C., 2007. Breakup of the Newfoundland–Iberia rift, in: Karner, G.D., Manatschal, G., Pinheiro, L.M. (Eds.), Imaging, Mapping and Modelling Continental Lithosphere Extension and Breakup, Geol. Soc. Lon. Spec. Pub. 282 9-46.

Tullis, J., Yund, R.A., 1985. Dynamics recrystallization of feldspar: A mechanism for ductile shear zone

formation. Geology 13 238-241.

Uyeda, S. Kanamori, H., 1979. Back-arc opening and the mode of subduction. J. Geophys. Res., 84, 1049-1061.

van Wijk, J.W., Cloetingh, S.A.P.L., 2002. Basin migration caused by slow lithospheric extension, Earth Planet. Sci. Lett. 198 275-288.

White, R., McKenzie, D., 1989. Magmatism at rift zones: The generation of volcanic continental margins and flood basalts. J. Geophys. Res. 94, 7685-7729.

Yamasaki, T., Gernigon, L., 2008. Styles of lithospheric extension controlled by underplated mafic bodies, Tectonophysics, in press, doi:10.1016/j.tecto.2008.04.024.

Yamasaki, T., Nakada, M., 1997. The effects of the spinel-garnet phase transition on the formation of rifted sedimentary basins. Geophys. J. Int. 130, 681-692.

Ziegler, P.A., Cloetingh, S., 2004. Dynamic processes controlling evolution of rifted basins. Earth Sci. Rev. 64, 1-50.

Figure captions

Fig. 1: Schematic figure of the one-dimensional model of lithospheric extension adopted in this study. Pure shear thinning is assumed for the entire lithosphere so that the vertical velocity of material is a linear function of depth. The applied extensional force F_a is assumed constant with time. The lithosphere is composed of three material layers: wet quartzite upper crust, anorthite lower crust and wet olivine mantle. The initial crustal thickness is t_c. The thickness of thermal lithosphere (a) is defined by the depth of the 1350 ℃ isotherm. The temperature at the upper and lower boundary of the model is 0 and 1350 ºC, respectively.

Fig. 2: Behaviour of viscosity coefficient B^* as a function of strain, following Eq. (7).

Fig. 3: Temporal evolution of (a)(b): strain rate ($\dot{\varepsilon}$), (c)(d): stretching factor (β) and (e)(f): tectonic subsidence (ζ) in the reference conventional model (RCM) for different F_as (TN/m). t_cs are (a)(c)(e): 30 km and (b)(d)(f): 40 km.

Fig. 4: Temporal evolution of $\dot{\varepsilon}$ for the strain hardening model (SHM) with t_c = 30 km, a = 90 km and F_a = 4.9 TN/m. Dependence of $\dot{\varepsilon}$ on (a) the strain ε_o required for the onset of strain hardening, (b) the factor δ controlling the increase in viscosity, and (c) the strain interval ΔE required for the completion of the hardening. Stress envelope at various time during the evolution of the model

with $\varepsilon_c = 0.6$, $\delta = 100$, $\Delta E = 0.8$ and $F_a = 4.9$ TN/m (Solid curve) is shown in (a). Stress envelope for the model without strain hardening (Dashed curve) is also depicted in the same figure, in which the ductile stress is evaluated using the strain rate predicted by the strain hardening model.

Fig. 5: Temporal evolution of (a) $\dot{\varepsilon}$, (b) β-factor and (c) ζ for SHM with $t_c = 30$ km and $a = 90$ km. Values of hardening parameters are: (I) $\varepsilon_o = 0.4$, $\Delta E = 0.7$, $\delta = 100$ and $F_a = 5.8$ TN/m, (II) $\varepsilon_o = 0.4$, $\Delta E = 0.7$, $\delta = 100$ and $F_a = 4.9$ TN/m, and (III) $\varepsilon_o = 0.1$, $\Delta E = 0.9$, $\delta = 2$ and $F_a = 4.9$ TN/m.

Fig. 6: Conditions of ε_o, δ and ΔE to obtain the failure mode of rifting. t_cs are (a) 30 km and (b) 40 km.

Fig. 7: The time (t_d) when the deceleration of $\dot{\varepsilon}$ is initiated as a function of ε_o for different δs. t_cs are (a) 30 km and (b) 40 km. F_as are (i) 4.9 TN/m, (ii) 5.5 TN/m and (iii) 6.0 TN/m for models with $t_c = 30$ km, and (i) 1.5 TN/m, (ii) 1.7 TN/m and (iii) 2.5 TN/m for models with $t_c = 40$ km.

Fig. 8: The duration of rifting (Δt_D) as a function of δ for different F_as and ΔEs. t_cs are (a) 30 km and (b) 40 km. ε_os are (i) 0.0, (ii) 0.3 and (iii) 0.6 for models with $t_c = 30$ km, and (i) 0.0, (ii) 0.5 and (iii) 0.9 for models with $t_c = 40$ km.

Fig. 9: Available stretching factor predicted by the SHM as a function of ε_o, δ and ΔE. F_a is beyond F_{cu}, and is restricted to be less than 6 TN/m. All results plotted in the figures are obtained by the model where the strain rate decreases to 10^{-17} (1/s) within 50 million years. t_cs are (a) 30 km and (b) 40 km.

Fig. A: Critical tectonic forces F_{cu} and F_{cl} in the RCM as a function of a for different t_cs. Shaded area indicates the range of currently accepted magnitude of tectonic force (e.g., Forsyth and Uyeda, 1975; Parsons and Richter, 1980; Bott et al., 1989; Bott, 1991; Schellart, 2004). F_{cu} is defined as the maximum tectonic force that results in failure mode of rifting. F_{cl} is defined as the minimum tectonic force that results in the initial strain rate greater than 10^{-17} (1/s).

Fig. B: The maximum ΔE that results in the failure mode of rifting as a function of F_a for different δs, where ε_o is held constant in each figure. Results are obtained by models with $F_{cu} < F_a \leq 6$ TN/m. Black and gray curves represent the results of the models with $t_c = 30$ and 40 km, respectively. Vertical dotted lines indicate F_{cu}. F_a less than that on each curve results in the failure mode of

rifting and vice versa.

Fig. C: The duration of rifting (Δt_D) as a function of δ for different ΔEs. ε_o is 0.0. **(a):** t_c is 30 km, and F_as are (i) 4.9 TN/m, (ii) 5.5 TN/m and (iii) 6.0 TN/m. **(b):** t_c is 40 km, F_as are (i) 1.5 TN/m, (ii) 1.7 TN/m and (iii) 2.5 TN/m.

Fig. D: Dependences of β-factor on ε_o, δ, ΔE and F_a. β-factor as a function of (a) ε_o, (b) δ and (c) F_a for different ΔEs. t_c is (i) 30 km and (ii) 40 km. The minimum value of ΔE is 0.0. The maximum value of ΔE is depicted in the figures.

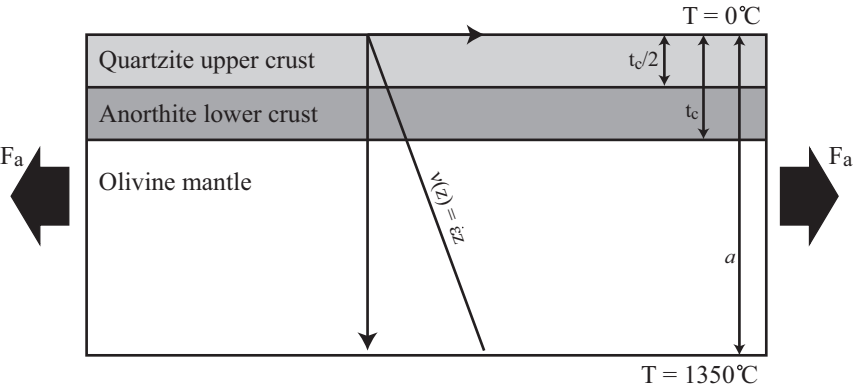

Figure 1

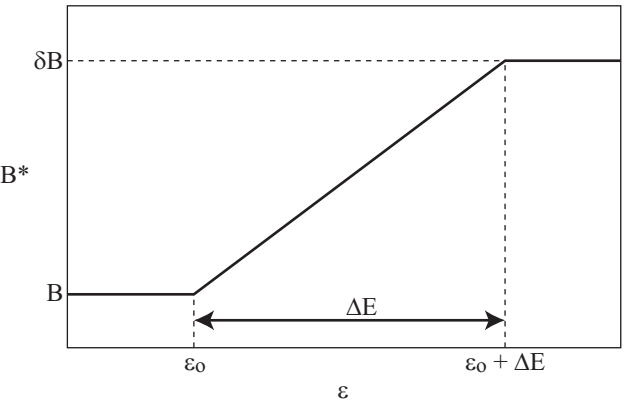

Figure 2

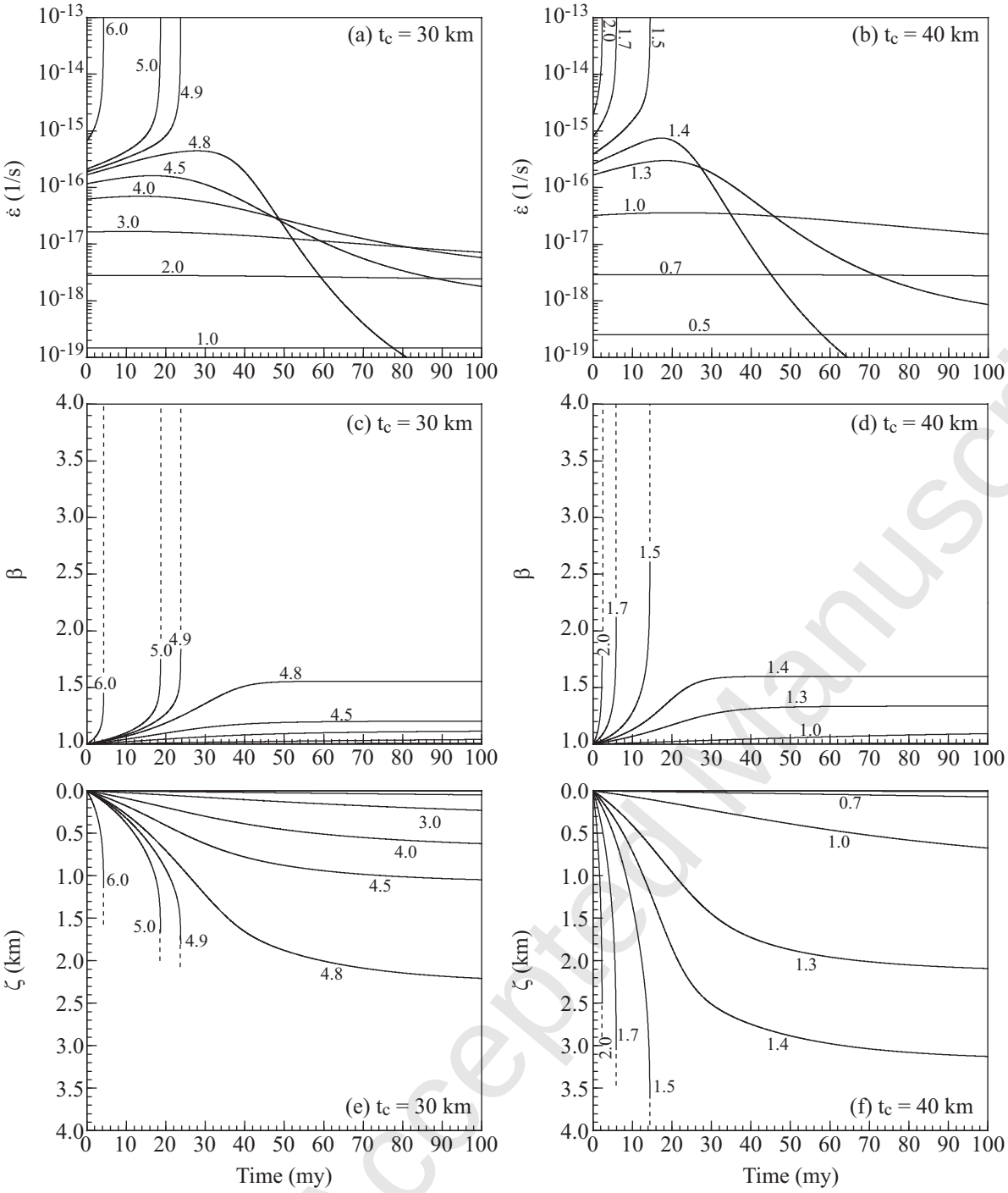

Figure 3

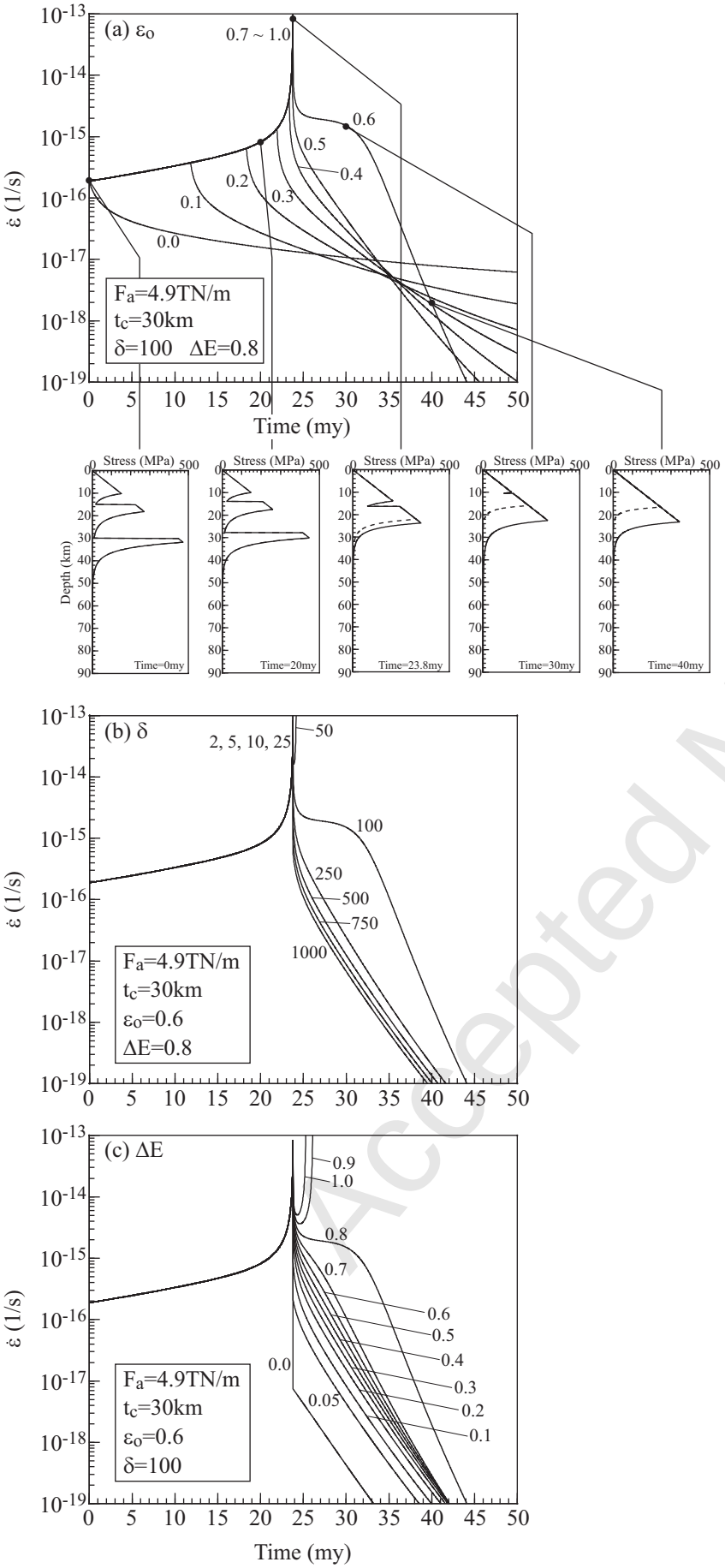

Figure 4

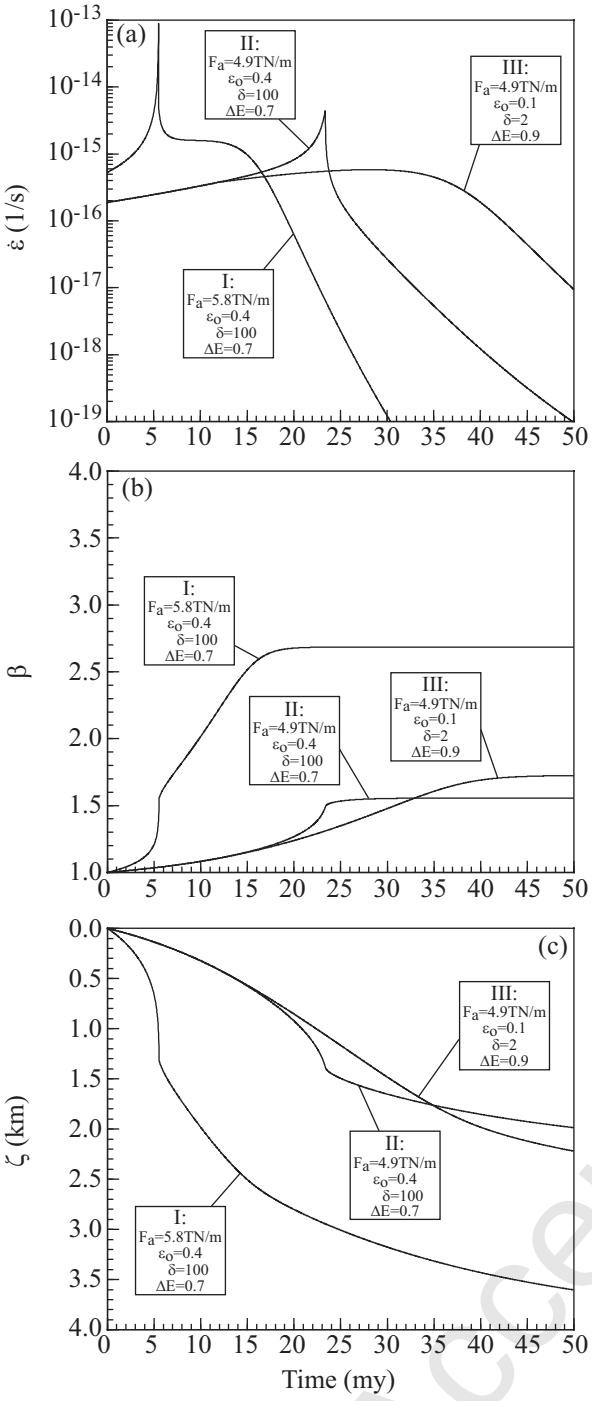

Figure 5

(a) t_c = 30 km

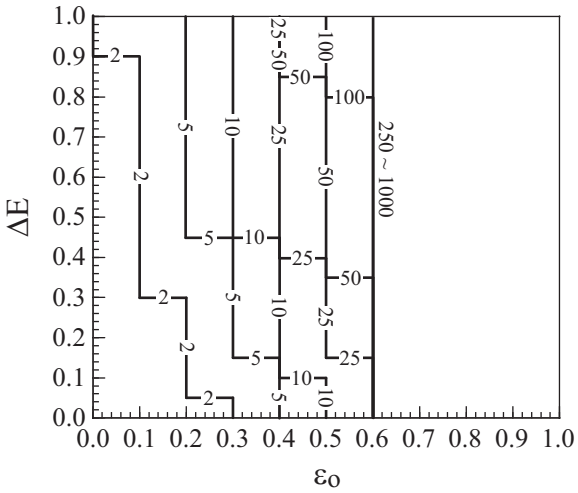

(b) t_c = 40 km

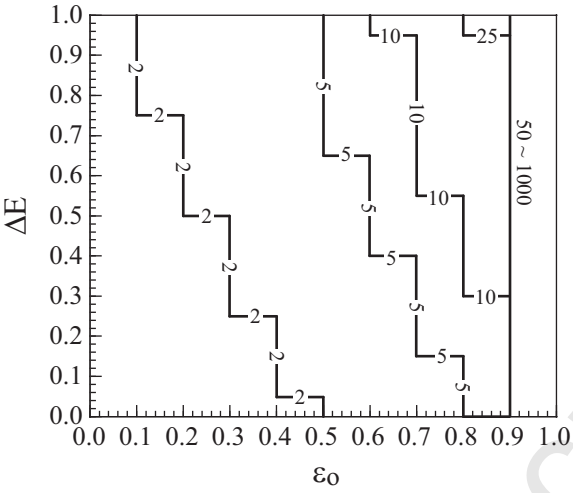

Figure 6

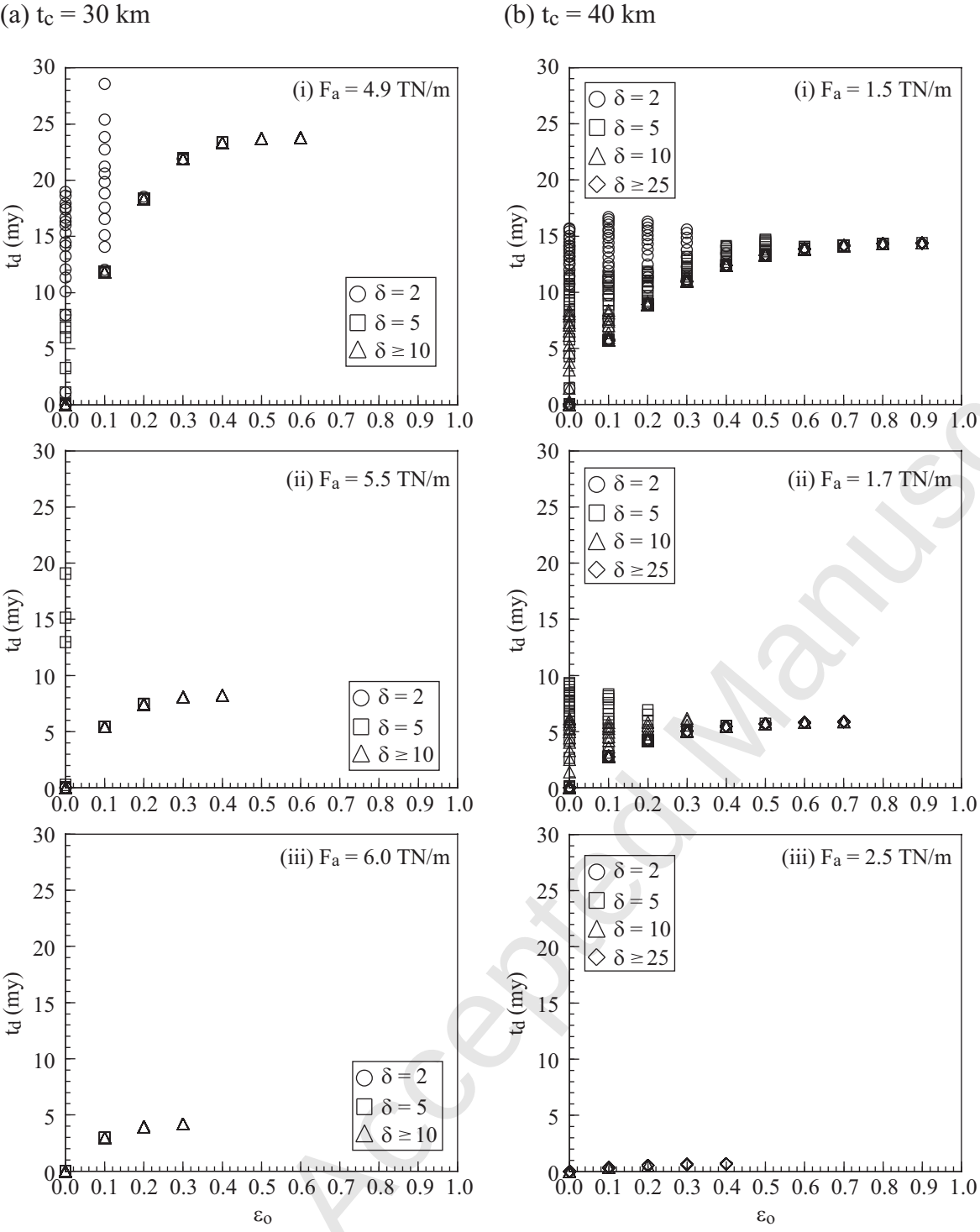

Figure 7

(a) t_c = 30 km (b) t_c = 40 km

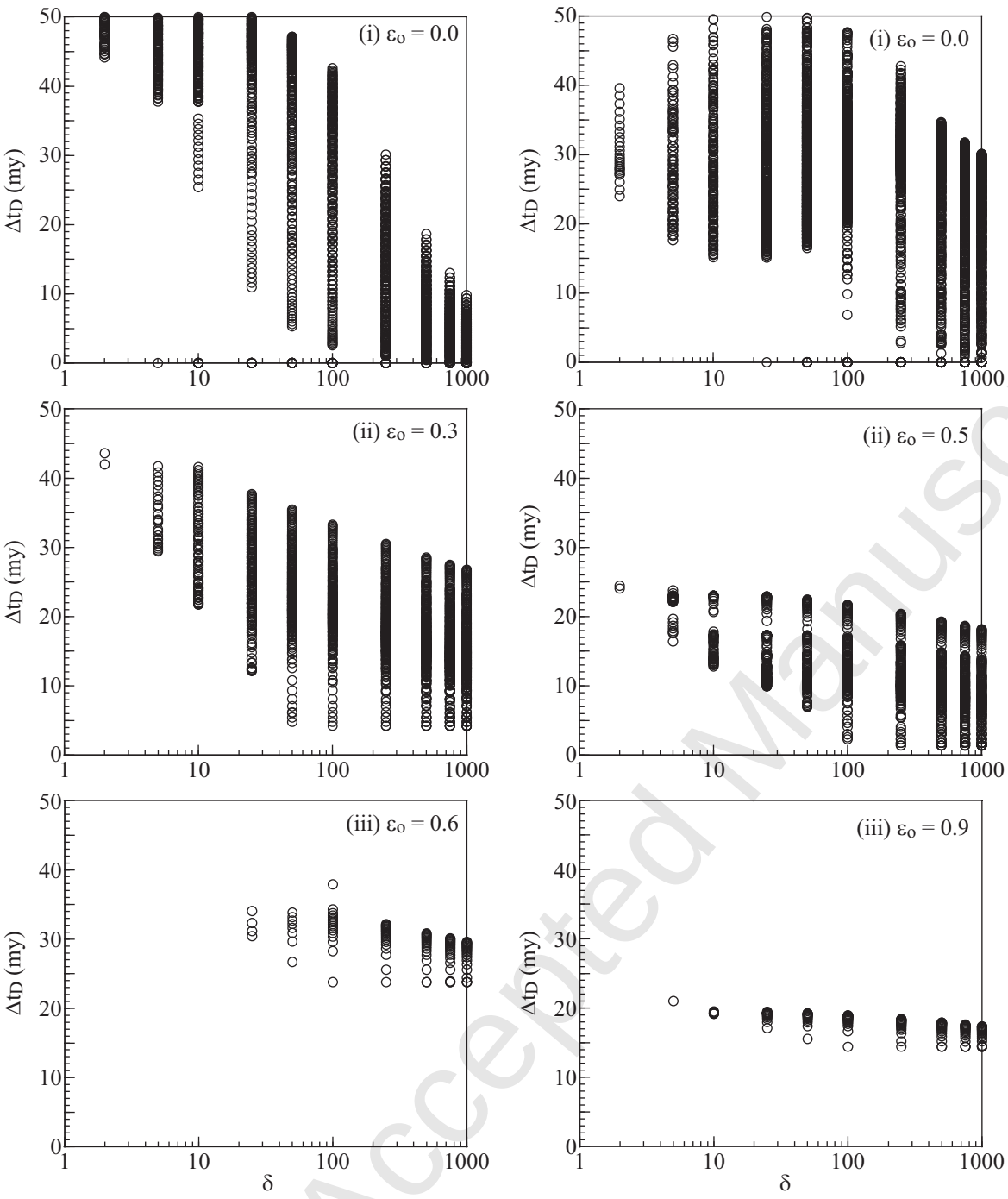

Figure 8

Figure 9

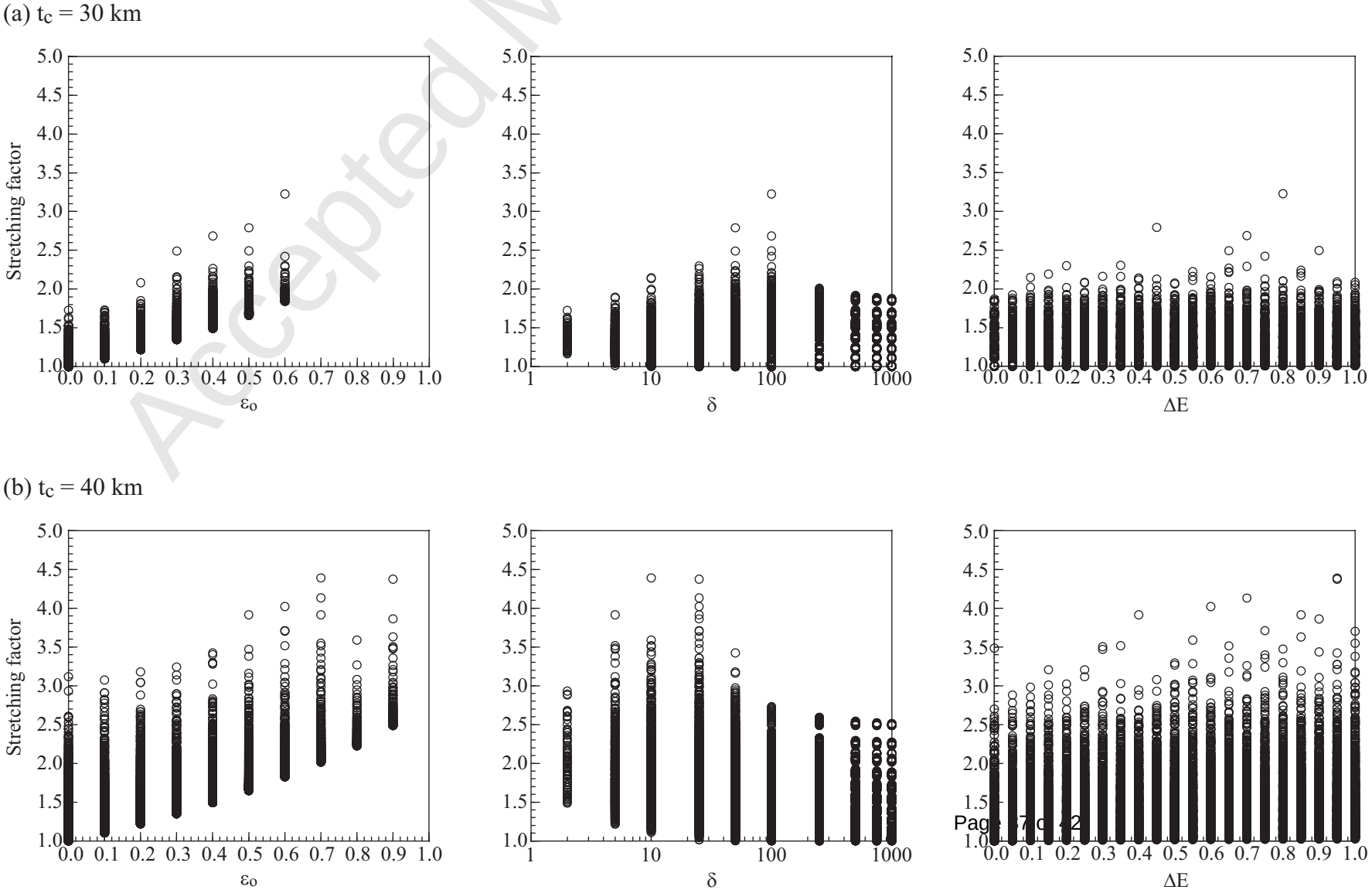

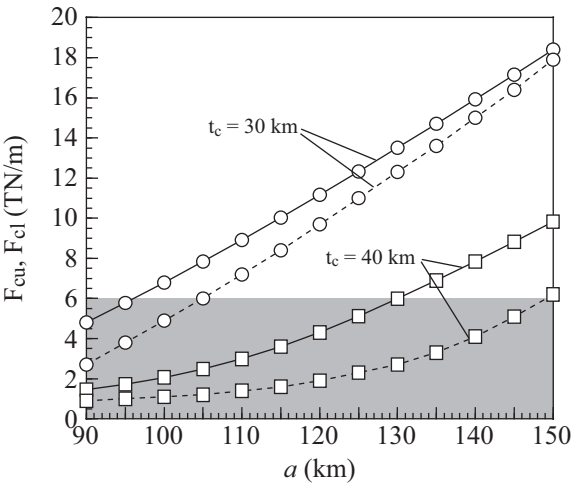

Figure A

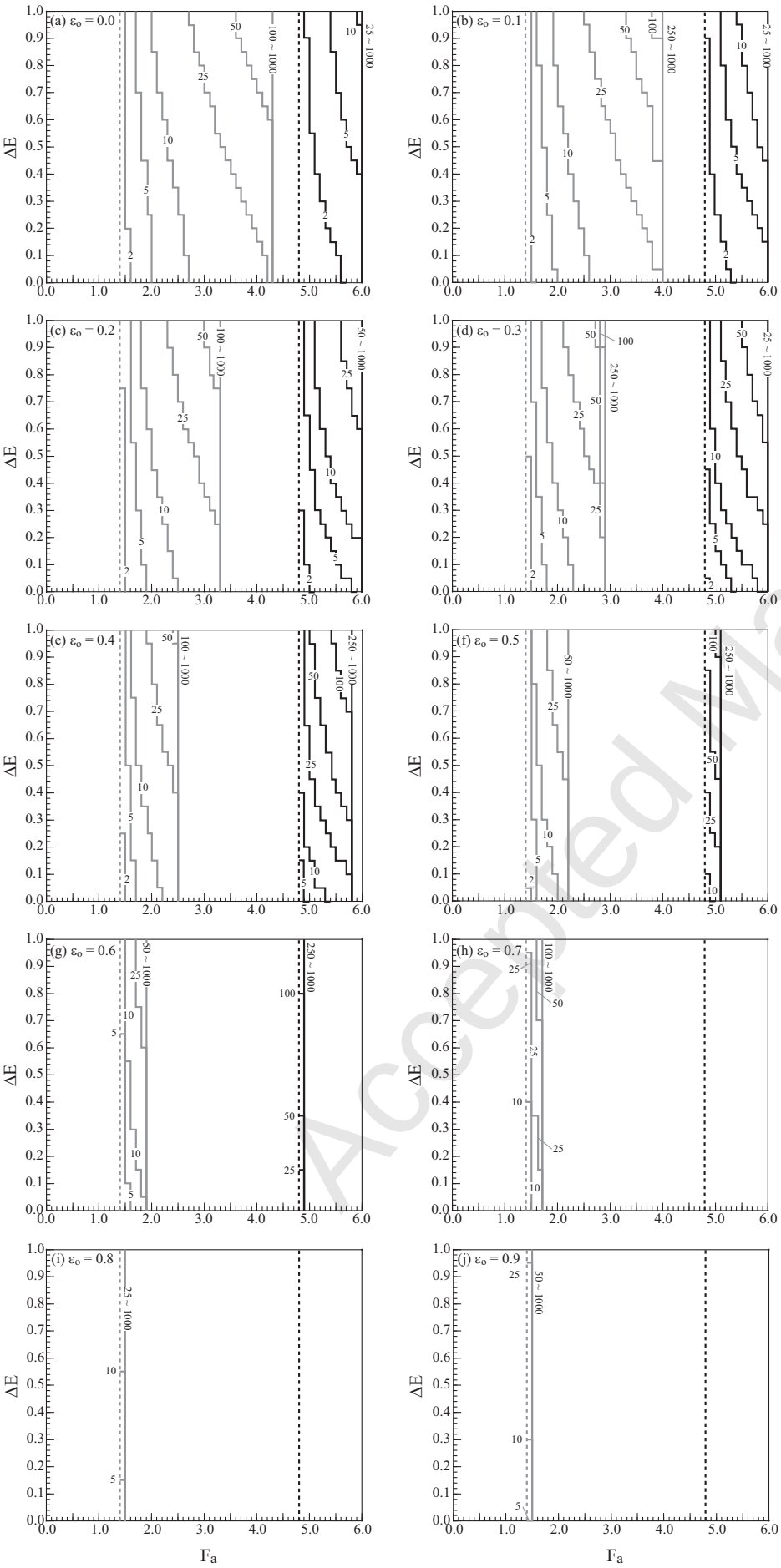

Figure B

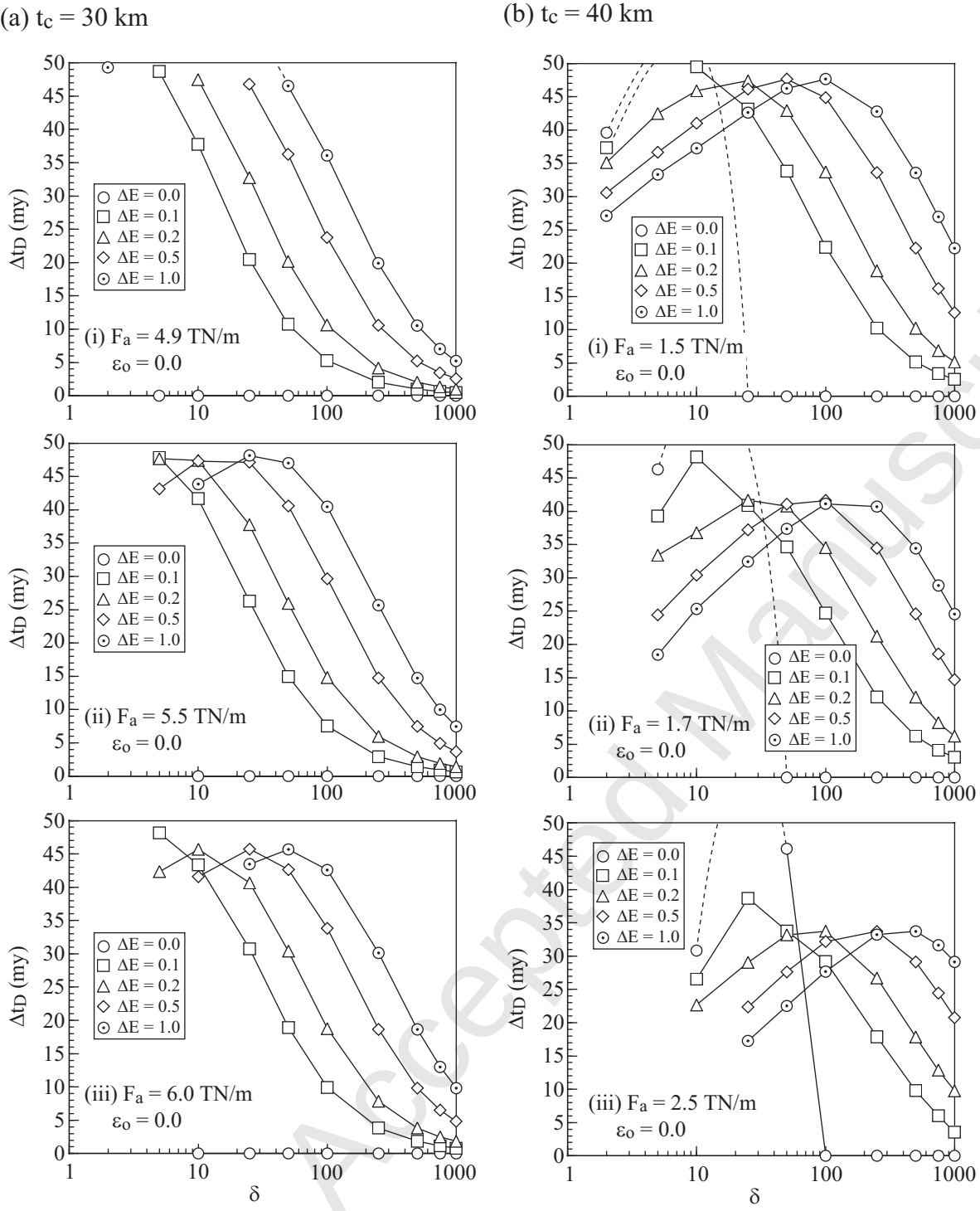

Figure C

(a) Dependence on ε_o

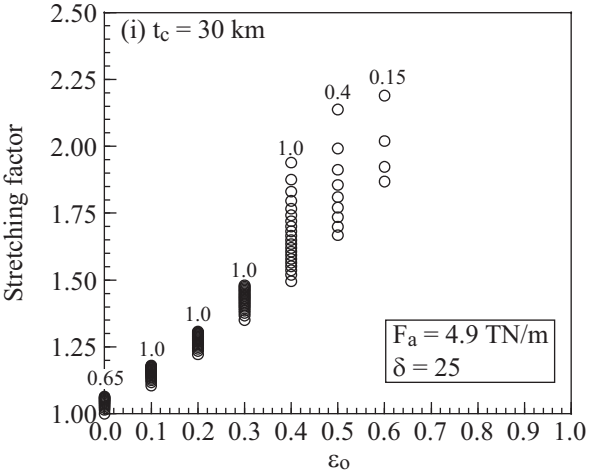

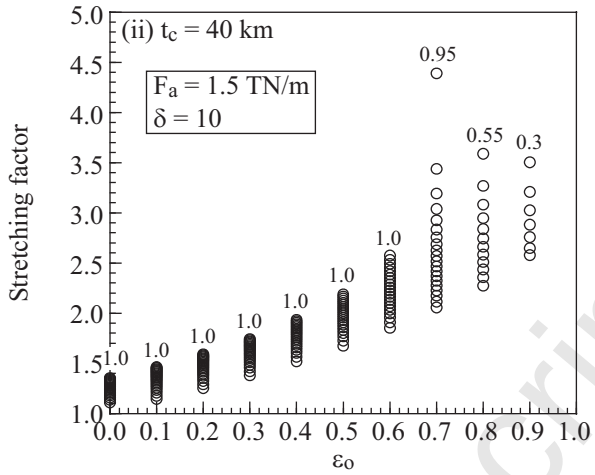

(b) Dependence on δ

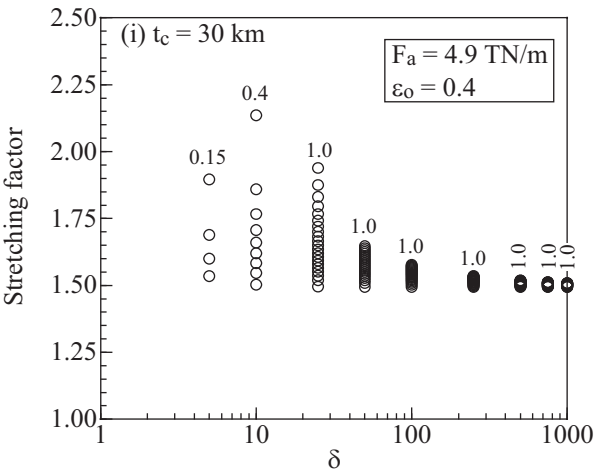

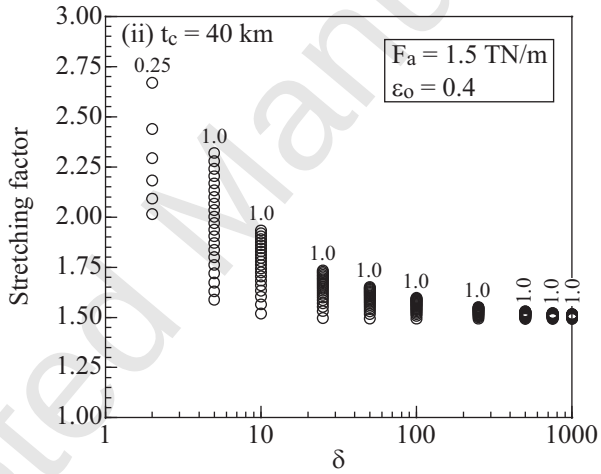

(c) Dependence on F_a

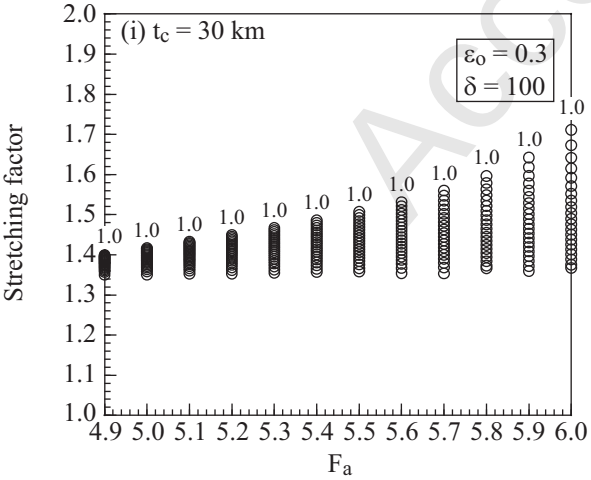

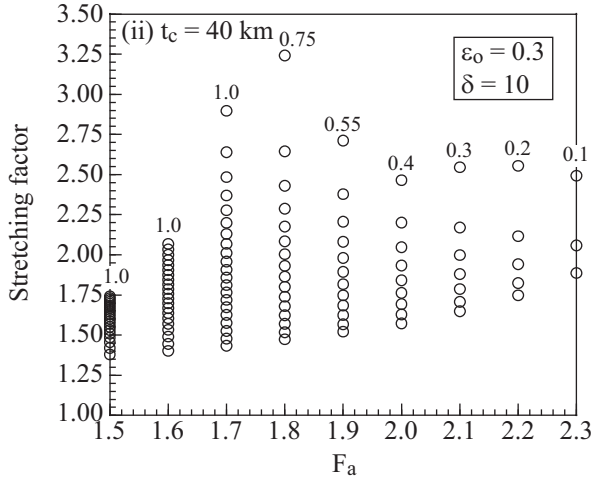

Figure D

Table 1: Model parameters used in this study

Symbol	Meaning	Value	Dimension
F_a	Tectonic force		TNm^{-1}
t_c	The initial thickness of the entire crust	30, 40	km
a	The initial thickness of the thermal lithosphere	90 - 150	km
σ_b	Brittle stress		Pa
ψ	Depth dependence of brittle failure	24	MPa/km
υ^*	Density ratio of pore water to rock	0.38	
z	Depth		m
σ_d	Ductile stress		Pa
ε	strain rate		s^{-1}
R	Universal gas constant	8.314	$Jmol^{-1}K^{-1}$
T	Temperature		ºC
Γ	Absolute temperature		K
t	time		s
κ	Thermal diffusivity	10^{-6}	m^2s^{-1}
ν	Vertical velocity of a material point		ms^{-1}
c	Specific heat	1050	$Jkg^{-1}K^{-1}$
ρ_{uc}	Mass density of the upper crust	2800	kgm^{-3}
ρ_{lc}	Mass density of the lower crust	2900	kgm^{-3}
ρ_m	Mass density of the mantle	3300	kgm^{-3}
ρ_w	Mass density of sea water	1010	kgm^{-3}
H	Heat production in the crust	0.647	mWm^{-3}
T_a	Potential temperature of the asthenosphere	1350	ºC
T_s	Temperature at surface	0	ºC
α	Coefficient of thermal expansion	3.0×10^{-5}	$ºC^{-1}$
S	Total strength of the thermal lithosphere		TNm^{-1}
F_{cu}	Upper critical tectonic force in the RCM		TNm^{-1}
F_{cl}	Lower critical tectonic force in the RCM		TNm^{-1}
F_{cush}	Upper critical tectonic force in the SHM		TNm^{-1}
β	Stretching factor		
ζ	Tectonic subsidence		m
ε_o	Strain required for the onset of hardening		
δ	Factor controlling the increase in viscosity		
ΔE	train interval required for the completion of hardening		
(Flow law parameters of power law creep)			
Wet quartzite: Koch et al. (1989)			
A^*_{uc}	Preexponent	1.10000×10^{-21}	$Pa^{-n}s^{-1}$
n_{uc}	Power	2.61	
Q_{uc}	Activation energy	145	$kJmole^{-1}$
Anorthite: Shelton and Tullis (1981)			
A^*_{lc}	Preexponent	5.60000×10^{-23}	$Pa^{-n}s^{-1}$
n_{lc}	Power	3.2	
Q_{lc}	Activation energy	238	$kJmole^{-1}$
Wet olivine: Karato et al. (1989)			
A^*_m	Preexponent	1.90000×10^{-15}	$Pa^{-n}s^{-1}$
n_m	Power	3	
Q_m	Activation energy	420	$kJmole^{-1}$